

1 **Congruent population genetic structures and divergence histories in anther-**
2 **smut fungi and their host plants *Silene italica* and the *S. nutans* species**
3 **complex**

4

5 **Running title:**

6 Co-structure of anther-smuts and their hosts

7

8 Fanny E. Hartmann¹, Alodie Snirc¹, Amandine Cornille², Cécile Godé³, Pascal Touzet³, Fabienne
9 Van Rossum^{4,5}, Elisabeth Fournier⁶, Stéphanie Le Prieur¹, Jacqui Shykoff¹, Tatiana Giraud¹

10

11 ¹ Ecologie Systématique Evolution, Bâtiment 360, Univ. Paris-Sud, AgroParisTech, CNRS,
12 Université Paris-Saclay, 91400 Orsay, France;

13 ² Génétique Quantitative et Evolution–Le Moulon, INRA; Univ. Paris-Sud, CNRS,
14 AgroParisTech, Université Paris-Saclay, 91198 Gif-sur-Yvette, France;

15 ³ Univ. Lille, CNRS, UMR 8198 - Evo-Eco-Paleo, F-59000 Lille, France;

16 ⁴ Meise Botanic Garden, B-1860 Meise, Belgium;

17 ⁵ Fédération Wallonie–Bruxelles, B-1080 Brussels, Belgium;

18 ⁶ UMR BGPI, Univ. Montpellier, INRA, CIRAD, Montpellier SupAgro, Montpellier, France;

19

20 * Author for Correspondence: Fanny E. Hartmann, Ecologie Systematique Evolution, Bâtiment
21 360, Univ. Paris-Sud, AgroParisTech, CNRS, Université Paris-Saclay, 91400 Orsay, France,
22 phone number : 01 69 15 72 82, e-mail address: fanny.hartmann@u-psud.fr

23

24 **Abstract**

25 The study of population genetic structure congruence between hosts and pathogens gives
26 important insights into their shared phylogeographic and coevolutionary histories. We studied the
27 population genetic structure of castrating anther-smut fungi (*Microbotryum* genus) and of their
28 host plants, the *Silene nutans* species complex, and the morphologically and genetically close *S.*
29 *italica*, which can be found in sympatry. Phylogeographic population genetic structure related to
30 persistence in separate glacial refugia has been recently revealed in the *S. nutans* plant species
31 complex across Western Europe, identifying several distinct lineages. We genotyped 171
32 associated plant-pathogen pairs of anther-smut fungi and their host plant individuals using
33 microsatellite markers and plant chloroplastic SNPs. We found clear differentiation between
34 fungal populations parasitizing *S. nutans* and *S. italica* plants. The population genetic structure of
35 fungal strains parasitizing the *S. nutans* plant species complex mirrored the host plant genetic
36 structure, suggesting that the pathogen was isolated in glacial refugia together with its host and/or
37 that it has specialized on the plant genetic lineages. Using random forest approximate Bayesian
38 computation (ABC-RF), we found that the divergence history of the fungal lineages on *S. nutans*
39 was congruent with the one previously inferred for the host plant and likely occurred with ancient
40 but no recent gene flow. Genome sequences confirmed the genetic structure and the absence of
41 recent gene flow between fungal genetic lineages. Our analyses of host-pathogen individual pairs
42 contribute to a better understanding of co-evolutionary histories between hosts and pathogens in
43 natural ecosystems, in which such studies are still scarce.

44
45 **Key words:** population genetic structure, host-pathogen interaction, cryptic speciation, genetic
46 divergence, approximate Bayesian computation, coevolution

47 **Introduction**

48 Host-pathogen interactions are pervasive in natural ecosystems, with many important ecological
49 and evolutionary consequences (Poulin, 2005; Thompson, 2005). Pairs of tightly interacting hosts
50 and pathogens may share common evolutionary histories due to co-evolution and/or shared
51 geographic and climatic constraints, or may follow distinct evolutionary trajectories due to
52 differences in reproductive systems, dispersal ranges, population sizes or contingent histories
53 (Tellier, de Vienne, Giraud, Hood, & Refrégier, 2010; Thompson, 2005). The comparison of
54 genetic divergence histories between host and pathogen populations gives important insights into
55 their shared phylogeographic history and possible local adaptation or host specialization (Croll &
56 Laine, 2016; Feurtey et al., 2016). Studies of phylogeny congruence of hosts and pathogens can
57 for example allow identifying host shifts or co-speciation events (de Vienne et al., 2013; Hafner
58 & Page, 1995; Wilson, Falush, & McVean, 2005). Several cases of host shift or co-speciation
59 events between hosts and pathogens have led to damaging diseases in plants, animals and humans
60 (Fisher, Gow, & Gurr, 2016; McDonald & Stukenbrock, 2016; Wolfe, Dunavan, & Diamond,
61 2007). The study of population genetic structure congruence within species or species complexes
62 can help identifying and understanding patterns of local adaptation (Gandon, Capowiez, Dubois,
63 Michalakis, & Olivieri, 1996), which play an important role in the dynamics of pathogen and host
64 communities (Gandon & Michalakis, 2002; Laine, 2005; Laine, 2008). Studies investigating the
65 congruence of population genetic structure and divergence histories between hosts and pathogens
66 are yet surprisingly still scarce despite their importance for understanding the evolutionary
67 mechanisms and histories leading to host specialization and local adaptation (Barrett, Thrall,
68 Burdon, & Linde, 2008; Croll & Laine, 2016), but see (Dybdahl & Lively, 1996; Feurtey et al.,
69 2016; McCoy, Boulinier, & Tirard, 2005; Michalakis, Sheppard, Noel, & Olivieri, 1993; Tsai &

70 Manos, 2010).

71 Anther-smut fungi (*Microbotryum* genus) are generally highly specialized on their host plant
72 species of the Caryophyllaceae family (Hartmann et al., 2019; Kemler, Göker, Oberwinkler, &
73 Begerow, 2006; Le Gac, Hood, Fournier, & Giraud, 2007; Refrégier et al., 2008) and patterns of
74 local adaptation have been reported in the system (Feurtey et al., 2016; Kaltz, Gandon,
75 Michalakis, & Shykoff, 1999). Therefore, they constitute a highly suitable system to study the
76 congruence of population genetic structure and divergence history between hosts and pathogens
77 at different evolutionary scales. Comparisons of phylogenies at the genus level suggested a
78 prevalence of host shifts at large evolutionary scales (Refrégier et al., 2008). The plant *Silene*
79 *latifolia* and its anther-smut fungus *M. lychnidis-dioicae* display strong congruence of population
80 genetic structures and plant local adaptation at regional and continental scales, suggesting the
81 existence of co-evolution in the system (Delmotte, Bucheli, & Shykoff, 1999; Feurtey et al.,
82 2016; Kaltz et al., 1999). Population genetic structures of both the host and the fungal pathogen
83 likely resulted from past climatic events, showing hallmarks of recolonization from former
84 glacial refugia in Europe (Badouin et al., 2017; Gladieux, Devier, Aguileta, Cruaud, & Giraud,
85 2013; Gladieux et al., 2011; Taylor & Keller, 2007; Vercken et al., 2010). The congruence of
86 host and pathogen population genetic structures has not been investigated in other anther-smut
87 fungi-*Silene* pairs despite their importance as models of pathosystems in natural ecosystems
88 (Bernasconi et al., 2009; Toh & Perlin, 2016) and the importance of assessing whether
89 congruence in population genetic subdivision is a general pattern (Croll & Laine, 2016).
90 Furthermore, the evolutionary history of population genetic divergence and of gene flow levels
91 occurring between pathogens infecting closely related hosts with overlapping distribution ranges
92 still remain poorly studied at the genome-wide-scale (but see Badouin et al., 2017).

93 *Silene nutans* is an assemblage of strongly differentiated cryptic genetic plant lineages,
94 corresponding to at least seven “evolutionary significant units”, which can be grouped into two
95 main phylogeographic (eastern and western) genetic clusters in Europe (Van Rossum et al.,
96 2018). The *S. nutans* genetic lineages display several morphological and ecological differences,
97 as well as nuclear and plastid genetic differentiation (Martin et al., 2016; Van Rossum et al.,
98 2018), and strong postzygotic reproductive isolation has been shown between the eastern and
99 western clusters in Western Europe (Martin et al., 2017). Geographic distribution patterns suggest
100 that *S. nutans* lineages have diverged in allopatry during the Quaternary climate oscillations, and
101 then recolonized northwards, without admixture (Martin et al., 2016; Martin et al., 2017; Van
102 Rossum et al., 2018). The anther-smut fungal species *Microbotryum violaceum sensu stricto* is
103 specialized on *S. nutans* (Kemler et al., 2006; Lutz et al., 2005). *Microbotryum* fungi are
104 pollinator-borne pathogens castrating plants by replacing the pollen by their own spores and
105 aborting ovaries, and they are usually highly specific on their *Silene* host plant species (Le Gac,
106 Hood, & Giraud, 2007; Refrégier et al., 2008). The existence of cryptic lineages within *S. nutans*
107 therefore raises the question of whether cryptic lineages also exist in the fungus and whether their
108 genetic divergence history mirrors that of the host. In Southern Europe, *S. nutans* can be found in
109 sympatry with *S. italica*, a closely related species, in particular in the Cévennes (Lafuma &
110 Maurice, 2006). *Silene nutans* and *S. italica* can be difficult to distinguish, being very similar
111 morphologically, mainly differing in petal shape, in the length of the gynophore and with rather
112 nodding or erect flowers, respectively (Rameau, Mansion, & Dumé, 1989, 2008; Tison & de
113 Foucault, 2014). Their flowering time, pollinator guilds and ecological niches overlap, although
114 they slightly differ in their ecological requirements, with *S. italica* being strictly calcicolous,
115 more xero-thermophilous and heliophilous than *S. nutans* (Rameau et al., 1989, 2008; Tutin et al.,
116 2001). *Microbotryum* fungi have been found on the two plant species and appeared differentiated

117 based on a small sample and a few genetic markers (Bucheli, Gautschi, & Shykoff, 2000);
118 however, spillover, i.e., non-sustainable cross-species disease transmission, has been shown to
119 occur in *Microbotryum* fungi (Antonovics, Hood, & Partain, 2002; Gladieux et al., 2011). The
120 study of the population genetic structure of *M. violaceum* s. s. on *S. nutans* therefore requires
121 molecular typing to check plant and fungal species identities.

122 In this study, we analyzed associated plant-pathogen samples of *S. nutans* and *S. italica*
123 populations from Europe in order to address the following questions: 1) Is there genetic
124 differentiation between anther-smut fungi parasitizing the closely related plant species *S. nutans*
125 and *S. italica*? Are there hybrids and/or spill-overs in anther-smut fungi? 2) Is the population
126 genetic structure of the anther-smut fungi parasitizing *S. nutans* and *S. italica* congruent with
127 those of their hosts? 3) What is the divergence history of these anther-smut fungi on their hosts?
128 Did genetic divergence occur with gene flow? Does the divergence history of the fungi mirror
129 that of their hosts? In order to address these questions, we used genetic markers (nuclear
130 microsatellite markers and/or chloroplastic SNPs) in both plants and anther-smut fungi to analyse
131 diseased material (171 plant-pathogen pairs) collected across Western Europe and infer
132 population genetic structures. We used approximate Bayesian computation (ABC) to compare
133 genetic divergence scenarios in anther-smut fungi in order to assess whether the genetic
134 divergence history in anther-smut fungi mirrored that inferred previously for their host plants. We
135 also sequenced 53 genomes of *Microbotryum* fungi and analysed them together with 46 available
136 *Microbotryum* genomes to assess whether the inferences on population genetic structure and gene
137 flow based on microsatellite markers hold at the genome-wide levels and whether there were
138 spill-overs or gene flow from other sympatric *Microbotryum* species than those analysed with
139 microsatellite markers.

140

141 **Materials and Methods**

142 **Fungal and plant materials**

143 We analyzed 171 anther-smut fungi collected from diseased plant individuals of *S. nutans* and *S.*
144 *italica* that were sampled in 55 distinct geographic sites across Europe, including the United
145 Kingdom, France, Belgium, Switzerland, Italy, Germany and Norway (Table S1, Fig. 1A).
146 Diseased plant individuals were stored in individual paper envelopes kept in plastic bags filled
147 with silica gel, in dark conditions at 8°C. Small pieces of leaves were used as raw material for
148 DNA extraction of host plant individuals. Diploid spores of *Microbotryum* anther-smut fungi
149 were collected in buds of infected flowers and grown as yeasts on potato dextrose agar (PDA)
150 medium, and then stored at -20°C. Spores did not grow for a few samples older than two years.
151 For DNA extraction of these strains, we used the dried spores directly collected from anthers of
152 diseased flowers. In most cases, spores from anthers of a single flower were used and therefore
153 corresponded to a single *Microbotryum* genotype (López-Villavicencio et al., 2007). When spore
154 material was limited, we used multiple anthers from several flowers of the same plant. We never
155 observed more than two alleles per strain and found low levels of heterozygosity per strain,
156 indicating that we unlikely genotyped more than one fungal genotype.

157

158 **Genotyping and identification of species and genetic lineages of the *Silene* plants based on** 159 **nuclear microsatellite markers and chloroplastic SNPs**

160 We extracted plant DNA of at least one diseased plant individual per site using the NucleoSpin®
161 96 Plant II kit (Macherey-Nagel, Germany). We obtained DNA for 134 out of the 171 diseased

162 plant individuals. At least one host individual was genotyped per site, except for six sites due to
163 the lack of plant material (Table S1). In addition, we genotyped three plant individuals for which
164 no anther-smut fungus was isolated but strains were isolated at the same sites (Table S1). Using
165 morphological criteria of the host plant species, sample collectors initially identified 153 *S.*
166 *nutans* and 18 *S. italica* diseased individuals. However, as the morphologies of *S. nutans* and *S.*
167 *italica* are very similar, misidentification could occur. Therefore, we sequenced four chloroplast
168 fragments (*psbA*, *LF*, *MATK*, *GS*; Lahiani et al., 2013) to check species identity of the diseased
169 plants collected in southeastern France and in Italy, where both *S. nutans* and *S. italica* can be
170 found. We thus reassigned one individual to *S. nutans* and seven individuals to *S. italica*, while
171 one host individual could not be assigned to either *S. nutans* or *S. italica* species (from the pair #
172 1436). We excluded this host-pathogen individual pair from our analyses. We thus had 145
173 diseased *S. nutans* plants and 25 diseased *S. italica* plant (Table S1).

174
175 To further genotype the plant individuals for studying the population genetic structure, we used a
176 combination of plastid (chloroplast) SNPs and nuclear microsatellite markers as previously
177 described (Godé et al., 2014; Martin et al., 2016; Martin et al., 2017). For plastid markers, using
178 the KASPAR® protocol we genotyped six SNPs, named Cp42, Cp397, Cp540, Cp656, Cp730
179 and Cp804, and polymorphic for [T/G], [A/C], [C/T], [G/T], [C/T], and [T/G], respectively.
180 Individual haplotypes were defined as combinations of allelic states for all six SNPs. For nuclear
181 markers, we used six multiplexes genotyping 24 microsatellite markers (Table S2). We followed
182 the previously published protocols (Godé et al., 2014; Martin et al., 2016; Martin et al., 2017),
183 except that we used different dye colors, bought from Eurofins Genomics. We used the Multiplex
184 PCR Kit (Qiagen) following manufacturer instructions for PCR reactions, performed separately
185 for each multiplex in 15 µL volume containing 3 µL of DNA, 3.4 µL of H₂O, 7.1 µL of multiplex

186 PCR Kit (Buffer 2X, Qiagen, USA), and 1.4 μ L of the primer mix. The primer mix included 2
187 μ M of unlabelled forward and reverse primers and 0.5 μ M or 0.75 μ M of the labelled forward
188 primer depending on the dye label. We used the same PCR cycling program as described in
189 (Godé et al., 2014) with some modifications of the final elongation for multiplex 1 (Table S3A-
190 C). We checked successful PCR amplifications on 2% (w/v) agarose gel electrophoresis. We
191 outsourced genotyping at the Gentyane Genotyping Platform (INRA, Clermont, France) and
192 scored alleles with GENEMAPPER v.4.0 (Applied Biosystems). We excluded three markers
193 (SIL18, SIL26, SIL42) for which we had less than 50% of the individuals successfully
194 genotyped. Given the material available, we could genotype 136 host plant individuals using both
195 plastid SNPs and nuclear microsatellite markers. All 136 genotyped host individuals had a
196 determined plastid haplotype and a determined genotype for at least 50% of the 21 remaining
197 nuclear microsatellite markers. The genotypes are deposited on Dryad (accession available upon
198 acceptance).

199
200 **Genotyping and species identification of the *Microbotryum* fungal strains: microsatellite**
201 **markers and ITS sequences**

202 We extracted fungal DNA using the Chelex protocol (Biorad, USA) following (Giraud, 2004).
203 We extracted DNA from the 170 strains of anther-smut fungi, either from mixes, stored at -20°C,
204 of haploid sporidia resulting from clonal growth after meiosis or from diploid teliospores directly
205 collected in anthers of diseased flowers and stored at 10°C. Diploid genomes were therefore
206 genotyped. DNA was diluted half-fold for PCR amplification. We used the internal transcribed
207 spacer (ITS) to check that the genus of the fungal strains belonged to the *Microbotryum* genus.
208 To genotype the fungal strains, we used 22 microsatellite markers arranged into multiplex (Table
209 S4 ; (Fortuna et al., 2016; Giraud et al., 2008)). We used the Multiplex PCR Kit (Qiagen)

210 following manufacturer instructions for PCR reactions which were performed separately for each
211 multiplex as described above. We used the PCR cycling programs as in previous studies (Fortuna
212 et al., 2016; Giraud et al., 2008; Table S3C-D). We checked the success of PCR amplifications on
213 2 % agarose gel electrophoresis. For genotyping, we pooled multiplexes 7 and 8 as a single
214 multiplex. We outsourced genotyping at the Gentyane Genotyping Platform (INRA, Clermont,
215 France) and scored alleles with GENEMAPPER v.4.0 (Applied Biosystems). We could
216 determine the genotypes for all strains for at least 50% of the 22 markers. We identified 21 fungal
217 strains that were likely siblings of other fungal strains based on null genetic distances and we
218 excluded them from the STRUCTURE software analyses (see below).

219

220 **Population genetic structure based on microsatellite markers**

221 To analyze and compare host and pathogen population genetic structures, we used a combination
222 of three complementary approaches using microsatellite nuclear markers on both the *Silene* host
223 plants and anther-smut fungal datasets. First, we used the model-based Bayesian clustering
224 approach implemented in the software STRUCTURE version 2.3.4 (Pritchard, Stephens, &
225 Donnelly, 2000). The program performs partitions of multilocus genotypes into genetic clusters
226 and assigns individuals to genetic clusters, minimizing the departure from expected frequencies
227 and linkage equilibrium among loci. We tested an admixture model with correlated frequencies
228 and no prior information for $K = 2$ to $K = 10$ clusters. A total of 10 repetitions were run for each
229 K value. We used 50,000 samples as a burn-in period and 100,000 samples per run for the Monte
230 Carlo Markov Chain (MCMC) replicates. Cluster assignment probabilities were computed using
231 the CLUMPP program (Jakobsson & Rosenberg, 2007) implemented in the R package
232 {Pophelper}. We used the R package {Pophelper} (<https://github.com/royfrancis/pophelper>) to
233 build the barplots. We choose as the biologically most relevant K value the finer population

234 structure, as the highest K value for which a new cluster could be identified with individuals
235 highly assigned to it, the new cluster at {K+1} having only admixed individuals (i.e. mean
236 membership coefficient <0.80 to the given cluster). For the anther-smut fungus dataset, genetic
237 data were haploidized as individuals were highly homozygous. High homozygosity levels might
238 bias inferences in the software STRUCTURE as these are based on Hardy-Weinberg expectations
239 in a diploid setting (Pritchard et al., 2000). Furthermore, 21 strains were removed, appearing as
240 siblings of other strains, with identical genotypes. *Microbotryum* fungi have one obligatory
241 sexual event before plant infection, so that clonemates cannot be found in different plants, but
242 high selfing rates may allow the same genotype to be found in neighbor plants if they are
243 parasitized by the same diploid spores or offspring (Giraud, 2004). For the host plant dataset,
244 genetic data were kept as diploid and five individuals were removed as they had identical
245 genotypes as other neighbor plants and may be clonemates. We identified clonemates and
246 siblings in both datasets using the dist(X) function in the R package {Ape} (Paradis, Claude, &
247 Strimmer, 2004) and considered two individuals to be siblings if their distance was equal to 0.
248 We then used two methods for assessing population genetic structure that do not assume
249 outcrossing or a lack of linkage disequilibrium. We performed a discriminant analysis of
250 principal components (DAPC) using the R package {ADEGENET} (Jombart, 2008; Jombart &
251 Ahmed, 2011) and used a principal component analysis (PCA) with the dudi.pca function using
252 the R package {ade4} (Dray & Dufour, 2007) on the entire set of individuals in both datasets.
253 Maps showing genotypes per locality were drawn using the R package {maps} (Becker, Wilks,
254 Brownrigg, Minka, & Deckmyn, 2017) and {mapplots} (Gerritsen, 2013). Scatter plots were
255 performed using the R package {ggplot2} (Wickham, 2009).

256

257 **Population statistics of genetic diversity and structure based on microsatellite markers**

258 We computed, using the R package {diveRsity} (Keenan, McGinnity, Cross, Crozier, & Prodöhl,
259 2016), the following estimates of genetic diversity per locus, site, genetic cluster identified in the
260 STRUCTURE analysis and/or species for the host plants and for the anther-smut fungi datasets:
261 the number of alleles, allelic richness (A_R), observed heterozygosity (H_O), expected
262 heterozygosity (H_E), the fixation indexes (F_{ST} , F_{IS} and F_{IT}), and the Jost's D statistics
263 corresponding to the fraction of allelic variation found among genetic clusters. We tested whether
264 genotype frequencies fitted the Hardy-Weinberg expectations using a standard χ^2 goodness of
265 fit method and assessed the significance of F_{ST} , F_{IS} and F_{IT} values using a bootstrap procedure
266 with 1000 iterations and calculating 95% confidence intervals. Sites with less than three sampled
267 individuals were pooled with other sites of the same genetic lineage when they were closer than
268 1/10th of latitude or longitude or were otherwise excluded from the analyses. We excluded nine
269 sites for the plants (site # 1014, 303, 1532, 719, 1546, 1547, 1437, 429, 1548, 1438) and 13 sites
270 for the fungal pathogens (site # 1068, 1014, 303, 1532, 719, 1546, 940, 1547, 1437, 333, 1249,
271 6809, 1548). In total, we considered 20 groups of sites for the host and 19 groups of sites for the
272 pathogen. We included sibling individuals but excluded individuals with admixed membership
273 between genetic clusters inferred from the STRUCTURE analysis (i.e. individuals with mean
274 membership coefficient <0.80 to the given cluster), which may be due to low assignment power
275 or admixture. To take into account differences of sample size between sites, we also estimated
276 allelic richness using ADZE (Szpiech, Jakobsson, & Rosenberg, 2008) which corrects for sample
277 size difference. Calculations were performed using a standardized sample size of $N=3$,
278 corresponding to the smallest number of observations per site. We tested for mean differences in
279 diversity statistics between species and genetic clusters using a Wilcoxon rank sum test and a
280 Kruskal-Wallis rank sum test in the R software v3.5.3, respectively, considering values across
281 groups of sites. To study isolation-by-distance patterns in the *S. nutans* and fungi parasitizing *S.*

282 *nutans* datasets, we computed correlations between matrices of genetic and geographic distances
283 of plant and fungal populations using a Mantel test. Genetic distances between populations at
284 each group of sites were calculated as the Nei's distance (Nei, 1972) using the `dist.genpop()`
285 function of the R package {ADEGENET} (Jombart, 2008; Jombart & Ahmed, 2011). Geographic
286 distances were calculated using the `dism()` function of the R package {geosphere}. We computed
287 Mantel tests using the `mantel.rtest()` function of the R package {ade4} with 1,000,000 resamples
288 for the null distribution. We also studied the correlations between matrices of genetic distances of
289 plant and fungal populations using a Mantel test as above. To remove the effect of the correlation
290 between genetic and geographic distances in the correlation between matrices of genetic
291 distances, we also performed a partial Mantel test using the `partial.mantel.test()` function of the R
292 package {ncf} with 1,000,000 resamples for the null distribution (Feurtey et al., 2016). We
293 considered 16 group of sites, the same both for the host and the pathogen, corresponding to *S.*
294 *nutans* host plants and fungal strains belonging to the genetic cluster parasitizing *S. nutans*. We
295 excluded sites of *S. italica* host plants and fungal strains belonging to the genetic cluster
296 parasitizing *S. italica*, and one site studied in the host but not studied in the pathogen (site # 333).
297 We investigated the occurrence of recent events of effective population size reduction (i.e.
298 bottlenecks) within the identified fungal genetic clusters using the program
299 BOTTLENECK version 1.2.02 (Piry, Luikart, & Cornuet, 1999).

300

301 **Inference of anther-smut fungi divergence history based on microsatellite markers**

302 We studied the divergence history of the anther-smut fungi sampled on the *S. nutans* lineage
303 complex using an approximate Bayesian computation-random forest (ABC-RF) procedure that
304 performs ABC inferences based on the machine learning tool named “random forest” (Breiman,

305 2001; Pudlo et al., 2016; Raynal et al., 2019). The divergence history of the host had already been
306 previously inferred (Martin et al., 2016; Martin et al., 2017; Van Rossum et al., 2018). To
307 increase our power to disentangle between different evolutionary scenarios, we performed model
308 choice and parameter estimation by comparing scenarios or groups of scenarios in sequential
309 rounds, each round testing a particular type of evolutionary event, either divergence time, order
310 of divergence or presence of gene flow (Estoup, Raynal, Verdu, & Marin, 2018; Liu et al., 2019);
311 Table 1; Table S5). We built scenarios based on the genetic clusters obtained using microsatellite
312 markers and on previous analyses of divergence of anther-smut fungi and their host species
313 (Badouin et al., 2017; Gladieux et al., 2013; Martin et al., 2016; Martin et al., 2017; Van Rossum
314 et al., 2018). The tested scenarios varied regarding the time of divergence, the relative order of
315 divergence of fungal genetic clusters and the occurrence of gene flow among genetic fungal
316 clusters (Table S5). We did not include scenarios with variation in effective population sizes as
317 the BOTTLENECK analysis did not identify any signature of effective population size reduction
318 (see 'Results' section). To test if the order of sequential rounds had an effect on the outcome of
319 the analysis, we tested the time of divergence and the relative order of divergence as either the
320 first or the second round (Note S1). We used as populations the fungal genetic clusters identified
321 through population structure analyses and removed fungal strains that were likely siblings of
322 other fungal strains in each genetic cluster.

323 We ran the ABC procedure modified from (Liu et al., 2019). Briefly, we simulated datasets with
324 22 fungal microsatellite markers using the ABCtoolbox program (Wegmann, Leuenberger,
325 Neuenschwander, & Excoffier, 2010) and used fastsimcoal 2.5 for coalescent-based simulations
326 (Excoffier & Foll, 2011). We simulated 10,000 genetic datasets per scenario using coalescent
327 simulations with model parameters drawn from prior distributions (Table S6A). We set prior

328 distributions based on previous analyses of divergence of anther-smut fungi and of their host
329 species (Badouin et al., 2017; Branco et al., 2018; Gladieux et al., 2013; Martin et al., 2016;
330 Martin et al., 2017; Van Rossum et al., 2018). We set a generation time of one year for the
331 pathogen based on its life cycle (Thrall, Biere, & Antonovics, 1993). We estimated the following
332 parameters: effective size of each genetic cluster (N), divergence time and migration rate per
333 generation between two genetic clusters x and y (T_{xy} and m_{xy} , respectively). We computed 16
334 summary statistics for the observed and simulated datasets with the program arlsumstats (Table
335 S6B; (Excoffier & Lischer, 2010). We assumed a generalized stepwise model of microsatellite
336 evolution (Estoup, Jarne, & Cornuet, 2002) and allowed the mutation rate to vary across
337 microsatellite markers. We drew locus-specific mutation rates from a gamma distribution ($\alpha, \alpha/\mu$)
338 in which μ is the mutation rate per generation and α is a shape parameter (Cornille et al., 2012;
339 Liu et al., 2019). We used the R package {abcrf} v1.7.0 (Pudlo et al., 2016) to compute a
340 classification vote through ABC-RF, representing the number of times a scenario was selected
341 among classification n trees of the constructed random forest. We chose $n=500$ trees. For each
342 round, we selected the scenario or group of scenarios with the highest number of classification
343 votes. We computed the posterior probability and the prior error rates over 10 replicated analyses.
344 We performed a linear discriminant analysis (LDA) in the R package {abcrf} v1.7.0 (Pudlo et al.,
345 2016) on the simulated and observed datasets to visually check the fit of the model to the
346 observed data. Finally, we performed parameter inferences using the group of models eventually
347 selected.

348

349 **Sequencing data and genome assemblies**

350 We performed whole-genome sequencing for 23 anther-smut fungal strains parasitizing *S. italica*

351 and 30 strains parasitizing *S. nutans*. Out of these 53 strains, 38 strains belonged to the 170 host-
352 pathogen pairs that were genotyped with microsatellite markers (Table S7). Due to limited fungal
353 material, we sequenced six additional strains that were collected at our studied sites but not
354 genotyped for microsatellite markers and nine additional strains collected at three new sites
355 (Table S7). We extracted DNA from fresh spores stored at -20°C using the Nucleospin Soil Kit
356 (Macherey-Nagel, Germany). Genomes were sequenced using Illumina 150 bp paired-end
357 sequencing technology at 46X coverage on average. We also included outgroups using available
358 whole-genome sequences of 56 anther-smut fungal strains parasitizing closely-related host
359 species of *S. nutans* and *S. italica* occurring in the studied geographic range (Le Gac, Hood,
360 Fournier, et al., 2007; Refrégier et al., 2008): 33 *M. lychnidis-dioicae* strains parasitizing *S.*
361 *latifolia* (Badouin et al., 2017), 19 *M. silenes-dioicae* strains parasitizing *S. dioica* (Badouin et al.,
362 2017) and four *M. violaceum* var *paradoxa* strains parasitizing *S. paradoxa* (Branco et al., 2018)
363 (Table S7). We downloaded raw data publicly available from the NCBI SRA under the
364 BioProject IDs PRJNA295022 and PRJEB16741. We thus analysed a total of 109 *Microbotryum*
365 genomes. For read mapping, we used as reference genome the high-quality haploid genome
366 assembly of the MvSn-1249 *M. violaceum* s. str. strain corresponding to the a₂ mating type
367 (collected on *S. nutans*) previously obtained with P6/C4 Pacific Biosciences SMRT technology
368 and annotated for gene models (Branco et al., 2017). The MvSn-1249-A2 assembly was accessed
369 from GenBank BioProject accession number PRJEB12080 (BioSample ID: SAMEA3706514,
370 assembly: GCA_900014965).

371

372 **Genome read mapping and variant calling procedure**

373 We performed read mapping and SNP calling of the 109 analysed genomes against the MvSn-
374 1249-A2 genome as previously described (Branco et al., 2018; Hartmann, Rodríguez de la Vega,

375 Brandenburg, Carpentier, & Giraud, 2018). First, we trimmed Illumina raw reads for sequence
376 quality and removed adapter sequences using the software Cutadapt v1.8.3 (Martin, 2011) with
377 the options: `-q 10, 10; --minimum-length 50; -a`
378 `AGATCGGAAGAGCACACGTCTGAACTCCAGTCAC;` `-`
379 `AAGATCGGAAGAGCGTCGTGTAGGGAAAGAGTGTAGATCTCGGTGGTCGCCGTATT.`
380 We aligned trimmed reads using the short read aligner bowtie2 v2.1.0 (Langmead, Trapnell, Pop,
381 & Salzberg, 2009) with the three following software options: `--very-sensitive-local; --phred33; -X`
382 `1000`. We removed PCR duplicates using the MarkDuplicates tool of Picard tools version 2.14.1
383 (<http://broadinstitute.github.io/picard>) and performed local realignment of mapped reads using
384 the tools RealignerTargetCreator and IndelRealigner of the Genome Analysis Toolkit (GATK)
385 version 3.8 (McKenna et al., 2010) to improve alignment accuracy in indel regions. Mean
386 alignment rates to the reference genome ranged from 53 to 96% (Table S7). For SNP calling, we
387 used GATK version 3.7 (McKenna et al., 2010) and ran HaplotypeCaller on each strain
388 individually using a diploid mode. Then, we used GenotypeGVCFs on a merged gvcf variant file
389 to perform joint variant calls. We filtered SNP calls for quality using VariantFiltration and
390 following the GATK good practices for hard-filtering of variants (`QUAL < 250; QD < 2; MQ <`
391 `30.0; -10.5 > MQRankSum > 10.5; -5 > ReadPosRankSum > 5; FS > 60; SOR > 3`) and masked
392 SNPs for repeats. We found 41 SNPs in the strain MvSn-1249-A2 (the very same fungal strain as
393 the reference genome also sequenced with Illumina), indicating low rates of false positives in our
394 SNP calling. We only kept bi-allelic SNPs with a high genotyping rate ($> 90\%$) on autosomes
395 (i.e., excluding SNPs on the mating-type contigs MvSn-1249-A2-R1_MC15 and MvSn-1249-A2-
396 R1_MC16). We excluded SNPs on the mating-type chromosomes for population genomics
397 analyses as they exhibit suppressed recombination on 90% of their lengths (Branco et al., 2018).
398 Removing the strain MvSn-1249-A2, we kept 108 fungal strains and 1,305,369 SNPs for

399 population genomic analyses.

400

401 **Population genomics analyses**

402 To analyze the population genetic structures of anther-smut fungi parasitizing several *Silene*
403 species using the genome-wide SNP dataset called on autosomes, we used the model-based
404 Bayesian clustering approach implemented in the software STRUCTURE version 2.3.4
405 (Pritchard et al., 2000), from K=2 to K=10 clusters, and performed a PCA, similarly as for the
406 microsatellite datasets. For the STRUCTURE analysis, we selected a set of 233 unlinked SNPs
407 randomly distributed at intervals of 100 kb along the autosomes, linkage disequilibrium decaying
408 over 50-100 kb in *Microbotryum* populations (Badouin et al., 2017). We used the R package
409 {Pophelper} (<https://github.com/royfrancis/pophelper>) to perform barplots. We performed the
410 PCA on all SNPs (but excluding missing data and heterozygote genotypes) using the --pca
411 command of the Plink v1.9 software (Chang et al., 2015; Purcell et al., 2007). To study footprints
412 of gene flow between fungal strains, we performed a phylogenetic network analysis implemented
413 in splitsTree (Huson, 1998; Huson & Bryant, 2006) with the neighborNet method.

414

415 **Results**

416 **Population genetic structure and diversity of *Silene nutans* and *S. italica* host plants**

417 After checking plant species identity with molecular markers, we retained 145 diseased *S. nutans*
418 plants and 25 diseased *S. italica* plants (Table S1; Fig 1A). The 21 plant nuclear microsatellite
419 markers distinguished well *S. nutans* and *S. italica* both in STRUCTURE analyses from K=2 and
420 in the principal component analysis (PCA; Fig 1B-C; Fig S1).

421 Within *S. nutans*, we identified four distinct haplotypes based on the six plastid SNPs, retrieving
422 in our sample the four major genetic lineages of *S. nutans* previously identified in Western
423 Europe (Fig 1A; (Martin et al., 2016; Martin et al., 2017; Van Rossum et al., 2018). The blue,
424 yellow, orange, and red haplotypes were found, as in previous studies, in the northeastern,
425 southeastern, western and southwestern parts of Europe, respectively. All *S. italica* samples had a
426 blue plastid haplotype (Fig 1A). Within *S. nutans*, the PCA based on the 21 plant nuclear
427 microsatellite markers mainly differentiated the orange genetic lineage from the other ones (Fig
428 1B; Fig S1B) and the STRUCTURE analysis detected four genetic clusters, corresponding to the
429 different plastid haplotypes, except for the red haplotype for which we had too few samples (Fig
430 1C; Fig S1A). The STRUCTURE analysis further identified two well-separated genetic clusters
431 within the *S. nutans* orange plastid haplotype (Fig. 1C). These two genetic clusters also appeared
432 separated on the second axis of the PCA and corresponded to plant individuals collected in the
433 Northern part of France *versus* Belgium and Western part of France (Fig S1), in agreement with
434 previous findings (Martin et al., 2016). From the STRUCTURE analyses, we identified five host
435 individuals with admixed cluster memberships (mean membership coefficient <0.80 to the given
436 cluster), which may be due to low assignment power or admixture between genetic clusters. We
437 found no further clear subdivision within *S. nutans* at higher K values and no clear population
438 subdivision within *S. italica* (Fig S1A).

439 We found no significant differences in allelic richness neither between *S. nutans* and *S. italica*
440 (Wilcoxon rank sum (WRS) test on 20 groups of sites, $W = 12$, p-value = 0.169; Table S8A) nor
441 between the four *S. nutans* genetic clusters (Kruskal-Wallis rank sum (KWRS) test on 16 groups
442 of sites, $\text{Chi}^2 = 4.92$, degree of freedom (df) = 3, p-value = 0.178; Table S8A). In *S. nutans*, levels
443 of observed heterozygosity were significantly lower than those of expected heterozygosity under

444 Hardy-Weinberg equilibrium for most loci, the mean F_{IS} value per marker being 0.33 (Table S2).
445 In *S. italica*, levels of observed and expected heterozygosities were not significantly different for
446 most markers (78%; Table S2), the mean F_{IS} value per locus being 0.37 (Table S2). As expected,
447 pairwise F_{ST} and Jost's D indicated higher divergence between *S. italica* and *S. nutans* (mean
448 F_{ST} =0.32; mean Jost's D=0.57; Table S9A) than between genetic clusters of *S. nutans* (mean
449 F_{ST} =0.20; mean Jost's D=0.35; Table S9A; KWRS test for both statistics, $W = 0$, p-value =
450 0.010). For *S. nutans*, we found on average lower pairwise F_{ST} and Jost's D values between the
451 yellow Western cluster and the two orange Western and Northwestern genetic clusters (mean
452 F_{ST} =0.17; mean Jost's D=0.28; Table S9A) than between the blue Eastern genetic cluster and the
453 Western genetic clusters (mean F_{ST} =0.24; mean Jost's D=0.42; Table S9A), although the
454 difference was not significant (KWRS test for F_{ST} , $W = 8$, p-value = 0.200; KWRS test for Jost's
455 D, $W = 9$, p-value = 0.100). The correlation between the matrices of pairwise genetic and
456 geographic distances for *S. nutans* (tested on 16 sites) was significantly positive (Mantel test: $r =$
457 0.54, p-value < 0.001), indicating an isolation-by-distance pattern.

458

459 **Differentiation between anther-smut fungi parasitizing *Silene nutans* and *S. italica***

460 Population genetic structure analyses separated *Microbotryum* strains into two main genetic
461 clusters, corresponding to their host plant of sampling, *S. italica* and *S. nutans*. The host of
462 collection separated strains according to the first axis of the PCA (Fig 2B). The STRUCTURE
463 analysis and the discriminant analysis of principal component (DAPC) also delimited two clear
464 fungal genetic clusters according to the host of sampling at $K=2$ (Fig 2C; Fig S2). In the PCA
465 (Fig. 2B), four *Microbotryum* strains sampled on *S. nutans* clustered with strains parasitizing *S.*

466 *italica* and one *Microbotryum* strain sampled on *S. italica* clustered with strains parasitizing *S.*
467 *nutans*. These strains may correspond to spill-overs, i.e. cross-species disease transmissions,
468 between the two studied *Silene* species or from other *Silene* species. We excluded for further
469 analyses the 11 strains that had their main cluster memberships < 80% in the STRUCTURE
470 analysis at K=2 (Fig 2C), which can be due to low assignment power or admixture.

471 Anther-smut fungi parasitizing *S. italica* had on average higher levels of allelic richness (WRS
472 test on 19 groups of sites, $W = 48$, $p\text{-value} = 0.004$) and observed heterozygosity (WRS test on
473 19 groups of sites, $W = 30$, $p\text{-value} = 0.014$) than anther-smut fungi parasitizing *S. nutans* (Table
474 S8B). Levels of observed heterozygosity were significantly lower than heterozygosity expected
475 under Hardy-Weinberg equilibrium for eight markers for *Microbotryum* fungi parasitizing *S.*
476 *nutans* and six markers for *Microbotryum* fungi parasitizing *S. italica* (Table S4).

477

478 **Similar genetic structure in anther-smut fungi as in their *Silene nutans* and *S. italica* host**
479 **plants**

480 The existence of additional levels of population genetic structure within fungal strains was
481 indicated by the STRUCTURE barplots (Fig S2), the second and third principal components of
482 the PCA that explained 27.9 % of the total variance between strains (Fig 2B). To investigate the
483 population structure within each of the two main genetic clusters of anther-smut fungi,
484 corresponding mainly to populations parasitizing *S. nutans* and *S. italica*, respectively, we
485 analyzed them separately, which confirmed the existence of a strong population structure within
486 anther-smut fungi parasitizing *S. nutans* (Fig 3A). The first two PCA axes separated fungal
487 strains into three distinct genetic clusters, corresponding to the three most frequent plastid

488 haplotypes identified in the host plant (Fig 3A), which was also supported by the DAPC and the
489 STRUCTURE analyses (Fig 3B; Fig S3). We named these three fungal genetic clusters the blue
490 Eastern, yellow Western and orange Western *Microbotryum* clusters, in reference to their *S.*
491 *nutans* host plastid haplotypes. In contrast to the host plant *S. nutans*, we found no clear
492 subdivision in the orange Western anther-smut fungal cluster (Fig S3). We found no genetic
493 clusters specific to strains sampled from a host with a red haplotype, perhaps due to the low strain
494 number. We excluded for further analyses the two admixed fungal strains (cluster memberships
495 <0.80 in a given cluster) and the three fungal strains sampled on a host with a red haplotype. We
496 found no further population structure in the set of 28 anther-smut strains parasitizing *S. italica*
497 (Fig S4), as for the host plant.

498 All three fungal genetic clusters parasitizing *S. nutans* had similar levels of allelic richness
499 (KWRS test on 16 groups of sites, $\text{Chi}^2 = 1.33$, $\text{df} = 2$, $\text{p-value} = 0.514$; Table S8B) and observed
500 heterozygosity (KWRS test, $\text{Chi}^2 = 0.67$, $\text{df} = 2$, $\text{p-value} = 0.716$; Table S8B). The F_{IS} varied
501 between genetic clusters from -0.11 to 0.82 (Table S8B). We found no significant differences in
502 differentiation between the three fungal genetic clusters (KWRS tests for F_{ST} and Jost's D , $\text{Chi}^2 =$
503 2 , $\text{df} = 2$, $\text{p-value} = 0.368$; Table S9B). The significant correlation between the matrices of
504 genetic and geographic distances between pairs of fungal populations parasitizing *S. nutans* (16
505 sites) indicated an IBD pattern (Mantel test: $r = 0.62$, $\text{p-value} < 0.001$). There was a significantly
506 positive correlation between genetic distance matrices for the fungal and the *S. nutans*
507 populations (16 sites; Mantel test: $r = 0.80$, $\text{p-value} < 0.001$), and it remained significant when
508 controlling for the IBD effect (partial Mantel test: $r = 0.70$, $\text{p-value} < 0.001$). Altogether, our
509 findings indicate strong congruence between the population genetic structures of the anther-smut
510 fungi parasitizing *S. nutans* and its host plant *S. nutans* (Fig 3C). We found no signatures of

511 recent reduction in effective population size in either of the three fungal genetic clusters
512 parasitizing *S. nutans* nor the fungal genetic cluster parasitizing *S. italica* using the
513 BOTTLENECK software (Piry et al., 1999) under either stepwise or two-phase models of
514 microsatellite evolution (Table S10; one-tailed Wilcoxon signed rank test, all P-values>0.36).

515

516 **Inferred divergence history of anther-smut fungi on *Silene nutans* congruent with of their**
517 **host plant**

518 To study if the anther-smut fungi on *S. nutans* shared the same history of divergence into cryptic
519 lineages as the one previously inferred for their host plants, the *S. nutans* cryptic species complex
520 (Martin et al., 2016; Martin et al., 2017; Van Rossum et al., 2018), we used an approximate
521 Bayesian computation random forest (ABC-RF) procedure. We compared various divergence
522 scenarios for the three identified *Microbotryum* genetic clusters parasitizing *S. nutans*. We
523 removed the 21 fungal strains that were likely siblings of other fungal strains, keeping 110
524 anther-smut fungal strains belonging to the blue Eastern, yellow Western and orange Western
525 *Microbotryum* genetic clusters parasitizing *S. nutans* and we used as outgroup the 25 genotyped
526 *Microbotryum* strains parasitizing *S. italica*.

527 We performed three rounds of scenario comparison, each testing a particular evolutionary event,
528 including divergence times, divergence order and the occurrence of gene flow (Table 1; Table S5;
529 Fig S5). At each round, we retained the inferred most likely evolutionary scenario to be used as
530 backbone for the subsequent rounds. To assess our power to discriminate between scenarios, we
531 checked posterior probability (Table 1) and assessed visually whether the observed data fell
532 within the clouds of simulated data of the compared scenarios (Fig S6).

533 In the first round ("time of divergence"; Table 1, "round 1"), we tested four different time periods
534 of divergence for various divergence orders (A, B or C; Fig S5A). The group of scenarios with
535 strongest support included a first divergence occurring between 100,000-1,500,000 years ago,
536 and a second divergence occurring between 0-20,000 years ago (posterior probability = 0.54 +/-
537 0.02, prior error rate = 34%; Table 1, "round 1"; Fig S6A). In the second round ("divergence
538 order"; Table 1, "round 2"), we found with a high posterior probability for the scenario assuming
539 a first divergence of the blue Eastern *Microbotryum* genetic cluster, followed by the divergence
540 between the yellow and orange Western *Microbotryum* genetic clusters (posterior probability =
541 0.79 +/-0.02, prior error rate = 2%; Table 1, "round 2"; Fig S6B). When testing the order of
542 divergence between clusters as first round and the time of divergence as second round, we
543 selected the same scenarios with a high posterior probability (Note S1; Table S11).

544 In the third round ("occurrence of gene flow"; Table 1, "round 3, step 1"), we compared in a first
545 step three groups of scenarios differing in the clusters affected by gene flow. The most supported
546 group of scenarios assumed gene flow among *Microbotryum* genetic clusters parasitizing *S.*
547 *nutans* but not with *S. italica* (posterior probability = 0.60 +/-0.02, prior error rate = 5%; Table 1,
548 "round 3, step 1"; Fig S6C). In the following steps (Table 1, "round 3, steps 2 to 4"), we
549 compared groups of scenarios of divergence with different timing of gene flow. Scenarios of
550 divergence with ancient gene flow were the most supported, which suggested that episodes of
551 ancient gene flow occurred during divergence or just following divergence of the three
552 *Microbotryum* genetic clusters parasitizing *S. nutans* and then completely stopped (posterior
553 probability = 0.76 +/-0.02, prior error rate = 35%; Table 1, "round 3, step 2"; Fig S6D-F).
554 However, we did not have enough power to differentiate between scenarios of ancient gene flow
555 that involved different genetic clusters (either all three genetic clusters or only the two Western

556 genetic clusters) or different times of past gene flow (either over a 0-20000 year period or a
557 50,000-500,000 year period; Table S5; posterior probability = 0.49 \pm 0.03, prior error rate = 60%;
558 Table 1, “round 3, step 5”). We performed parameter inferences for the group of four models
559 with ancient migration (“round 3, step 2”, group 3 see Table 1; Table S12). The inferred dates
560 and order of divergence between fungal genetic clusters parasitizing *S. nutans* were consistent
561 with the history of divergence previously inferred for the host plant *S. nutans* (Fig 4; Martin et
562 al., 2016; Martin et al., 2017; Van Rossum et al., 2018).

563

564 **No genome-wide signatures of gene flow between anther-smut fungi on distinct *Silene***
565 **species**

566 To check whether genome-wide data support the patterns inferred above on population genetic
567 structure in the anther-smut fungi and lack of recent gene flow, we sequenced the genomes of 53
568 *Microbotryum* strains parasitizing *S. nutans* or *S. italica* (Table S7). We also used previously
569 sequenced genomes of anther-smut fungi parasitizing species with overlapping geographical
570 ranges in order to check if some of the strains that appeared as admixed or did not cluster
571 according to their host species may actually correspond to other *Microbotryum* species. After
572 filtration, we obtained 1,305,369 SNPs for 108 *Microbotryum* strains. We performed PCA
573 analyses on the genome-wide SNPs and STRUCTURE analyses and confirmed strong population
574 differentiation between fungal strains parasitizing *S. nutans* and *S. italica* (Fig 5A-B; Fig S7A).
575 Only one strain parasitizing *S. nutans* clustered with strains parasitizing *S. italica*, similarly as
576 found from microsatellite data (strain # 1438; Fig 2C), therefore likely being a genuine spill-over
577 between *S. nutans* and *S. italica*. Two other strains parasitizing *S. nutans* clustered with strains

578 parasitizing *S. latifolia*. These strains had admixed cluster membership (i.e. mean membership
579 coefficient <0.80 to the given cluster) or clustered with strains parasitizing *S. italica* from
580 microsatellite data (Fig 2C). These strains likely represent spill-overs between *S. nutans* and *S.*
581 *latifolia*.

582 Genome sequences retrieved the same genetic structure as microsatellites for anther-smut fungi
583 parasitizing *S. nutans*, with a strong differentiation between *Microbotryum* strains sampled on the
584 *S. nutans* blue plastid haplotype on the one hand and those sampled on yellow, red or orange
585 plastid haplotypes on the other hand (Fig S7B), and confirmed the absence of strong population
586 structure within anther-smut fungi parasitizing *S. italica* (Fig S7C). We also found strong
587 population differentiation between fungal strains parasitizing the three closely related host
588 species of *S. nutans* and *S. italica* (Fig 5A-B). STRUCTURE analyses showed no signatures of
589 recent admixture between strains parasitizing different hosts (Fig 5B).

590 The phylogenetic network analysis implemented in SplitsTree also supported the absence of
591 recent gene flow at the genome-wide levels between the *Microbotryum* species parasitizing
592 different hosts and the close genetic similarity of the three genetic clusters of anther-smut fungi
593 parasitizing the *S. nutans* complex (Fig 5C). Within *Microbotryum* strains parasitizing *S. nutans*,
594 we found no footprint of recombination between strains of the two main genetic clusters (Fig 5C)
595 which was consistent with a scenario of divergence with ancient migration and no contemporary
596 gene flow inferred from ABC demographic inferences.

597

598 **Discussion**

599 We found that genetic structure and divergence history of anther-smut fungi parasitizing the *S.*
600 *nutans* plant species complex closely mirrored those of their host plant genetic lineages. Such a
601 congruence in population structure and divergence history of the host and the pathogen in the *S.*
602 *nutans* complex, the distribution area of the genetic clusters in Western Europe, as well as the
603 inferred dates of divergence suggest that the host and the pathogen differentiated in parallel
604 following isolation in shared glacial refugia. To confirm the co-divergence events between *S.*
605 *nutans* lineages and anther-smut fungi genetic clusters, we need to more accurately date the node
606 of lineage divergence events in the host and the pathogen. Such molecular dating is essential to
607 support co-divergence events as preferential shifts of the pathogen to closely related host species
608 can also produce congruent phylogenies (de Vienne et al., 2013), but is currently difficult due
609 lack of appropriate calibration points.

610 Nevertheless, our results rule out the hypothesis that anther-smut fungi on some of the *S. nutans*
611 genetic lineages may result from specialization by host shifts from distant anther-smut fungi
612 parasitizing other *Silene* species in sympatry or parapatry. This contrasts with the prevalence of
613 host shifts between distant lineages observed in the Caryophyllaceae-*Microbotryum* system at
614 larger evolutionary scales (Refrégier et al., 2008), but is consistent with the strong congruence
615 reported between the population genetic structures of *S. latifolia* and its anther-smut fungi, also
616 corresponding to glacial refugia footprints (Feurtey et al., 2016). Our study thus contributes to
617 gain general insights into the processes of divergence in host-pathogen systems. While at large
618 evolutionary scales, host shifts seem to be the rule (de Vienne, Hood, & Giraud, 2009; Thines,
619 2019), finer and more recent population subdivisions may more often result from codivergence
620 due to shared geographic and climatic constraints, such as glacial refugia. The discrepancy
621 between the two evolutionary scales may be due to recurrent pathogen lineage extinctions

622 followed by recolonizations through host shifts: codivergence may occur frequently, but
623 pathogen lineages would regularly go extinct over longer evolutionary scales and plant lineages
624 would be recolonized by host shifts. This novel hypothesis can be tested by studying further
625 closely related pairs of natural host-pathogen associations, which unfortunately still remain
626 scarce.

627 The significant IBD pattern in both the *S. nutans* plant and anther-smut fungi and the correlation
628 between the genetic distances between host and pathogen pairs when controlling for IBD suggest
629 that the anther-smut fungi followed similar recolonization routes as the plant and/or became
630 specialized on the host genetic lineages. However, contrary to the system *S. latifolia* - *M.*
631 *lychnidis-dioicae* (Feurtey et al., 2016) and other host-pathogen systems (Barrett et al., 2008;
632 Criscione, Poulin, & Blouin, 2005; Nieberding et al., 2008; Nieberding & Olivieri, 2007), we
633 found higher levels of subdivision in *S. nutans* than in its associated anther-smut fungi. The
634 weaker genetic structure in anther smut fungi compared to its host suggests again extinction of
635 the pathogen lineage in a plant lineage, followed by recolonization from another fungal lineage,
636 or the ability of an anther-smut lineage to remain generalist on two closely related plant lineages.

637 Future studies using cross-inoculation experiments between strains and host plants of different
638 genetic clusters within the *S. nutans* complex could assess whether the congruence of host-
639 pathogen genetic structure is associated with a pattern of local adaptation of the pathogen or of
640 the pathogen, as in the system *S. latifolia* - *M. lychnidis-dioicae* (Delmotte et al., 1999; Feurtey et
641 al., 2016; Kaltz et al., 1999). We could not obtain enough fresh material for this study to be able
642 to test local adaptation. Furthermore, strong asymmetric postzygotic reproductive isolation was
643 found between the Eastern and Western *S. nutans* plant lineages (Martin et al., 2017) and it would
644 be interesting in future studies to explore if a similar reproductive isolation pattern is present

645 between the Eastern and Western fungal lineages on *S. nutans*, and whether reproductive
646 isolation can be found among anther-smut fungi.

647 We found clear differentiation between fungal populations parasitizing the two closely related *S.*
648 *nutans* and *S. italica* species, supporting previous findings of differentiation based on a few
649 strains and loci (Bucheli et al., 2000). No strong population structure was found within *S. italica*
650 or within its associated anther-smut fungi. However, future studies with larger sampling
651 distribution in the *S. italica* range in the Mediterranean Basin (Naciri, Pasquier, Lundberg,
652 Jeanmonod, & Oxelman, 2017) may identify population differentiation. Cross-species disease
653 transmissions, i.e. spill-overs of fungal strains, were more frequent on *S. nutans* than on *S. italica*,
654 which may be due to unequal sampling size between the two *Silene* species or to biological
655 differences. Some Caryophyllaceae plants indeed seem more susceptible to cross-species
656 transmissions (Antonovics et al., 2002; de Vienne, Hood, et al., 2009; Hood et al., 2019). Putative
657 spill-overs may actually correspond to other *Microbotryum* species, that were too rare to be
658 identified in our population analyses using microsatellite markers, as revealed with the whole
659 genome sequence data. In fact, two strains collected on *S. nutans* were actually assigned, based
660 on whole genome sequences, to *M. lychnidis-dioicae*, specialized on *S. latifolia*.

661 The statistical comparison of demographic models and the whole-genome SNP analyses indicated
662 the absence of recent gene flow between *Microbotryum* species parasitizing closely related *Silene*
663 species, as well as between the Eastern and Western fungal lineages parasitizing *S. nutans*,
664 although some spill-over cases were detected. Noteworthy, we also found no evidence of hybrid
665 individuals between the two host plants species *S. nutans* and *S. italica* based on SNP data. The
666 admixed barplots observed in the microsatellite STRUCTURE analyses must therefore have been
667 due to low power of assignment rather than recent hybridization. This result was consistent with

668 previous studies on other several anther-smut fungi, in which no hybrids were detected in natural
669 populations, even between very closely related species that can hybridize in the laboratory
670 (Abbate et al., 2018; Badouin et al., 2017; Gladieux et al., 2013; Petit et al., 2017). The only case
671 where hybrids were detected was among closely related anther-smut fungi with overlapping host
672 and geographic ranges, on *Dianthus* species (Petit et al., 2017). Ecological factors, such as
673 different habitats, pollinator guilds or flowering time of the host species (Jürgens, Witt, &
674 Gottsberger, 1996; Kephart, Reynolds, Rutter, Fenster, & Dudash, 2006), may constitute pre-
675 zygotic factors favoring reproductive isolation of host-specialized anther-smut fungi in natural
676 populations. Both extrinsic and intrinsic post-zygotic barriers can be strong in anther-smut fungi
677 (Giraud & Gourbière, 2012; Le Gac, Hood, & Giraud, 2007). Strong host specialization may
678 indeed play a role in reproductive isolation, through migrant inviability and hybrid maladaptation
679 on parental hosts, especially given the life cycle of *Microbotryum* fungi, with many spores falling
680 on a plant and competing for systemic infection, and selfing being frequent, exposing hybrids to
681 systematic competition with non-hybrids (Gibson, Hood, & Giraud, 2012). In addition,
682 comparative genomics of anther-smut fungi showed presence of large genomic rearrangements
683 and gene content variation between species (Branco et al., 2018; Hartmann et al., 2018), and
684 experimental crosses suggested high frequency of hybrid sterility and abnormal genomic contents
685 in hybrids (de Vienne, Refrégier, et al., 2009).

686 The low levels of gene flow among anther-smut fungi parasitizing different hosts found in
687 *Microbotryum* fungi stand in high contrast with frequent reports of signatures of introgression in
688 other fungal pathogens, such as crop pathogens or human disease-associated pathogens (Feurtey
689 & Stukenbrock, 2018). Few studies have focused on fungal pathogens diversification in natural
690 host communities while several evolutionary processes, such as time scale of divergence, host

691 density and heterogeneity, are likely very different than those occurring on human-modified
692 environment pathogens (Laine, 2005; Laine, Barrès, Numminen, & Siren, 2019; Stukenbrock &
693 McDonald, 2008). To understand how biodiversity arises and what the mechanisms of host-
694 pathogen evolution are over large evolutionary scales, we need more studies on co-evolutionary
695 histories of parasites and their hosts in natural ecosystems. Studies of population genetic structure
696 and divergence in plant fungal pathogens indeed remain so far mostly focused on crop pathogens
697 (Barrès et al., 2008; Enjalbert, Duan, Leconte, Hovmøller, & De Vallavieille-Pope, 2005;
698 Fournier & Giraud, 2008; Linde, Zhan, & McDonald, 2002; Saleh, Milazzo, Adreit, Fournier, &
699 Tharreau, 2014; Stukenbrock, Banke, & McDonald, 2006; Zaffarano, McDonald, & Linde,
700 2008), in which patterns are heavily impacted by host genetic homogeneity and high abundance,
701 as well as by human-mediated plant and pathogen dispersal. We found here strong population
702 structure congruence between hosts and pathogens, in agreement with a previous study on other
703 anther-smut lineages (Feurtey et al., 2016). Further studies on other natural systems are needed to
704 assess whether this represents a general pattern in natural pathogen-host communities.

705

706 **Acknowledgements**

707 We thank all the collectors cited in Table S1 and S7 for their contribution to plant material
708 sampling, the Département de la Nature et des Forêts (Service Public de Wallonie, Belgium), B.
709 Clesse (Centre Marie-Victorin, Cercles des Naturalistes de Belgique asbl), Ardenne & Gaume
710 and Natagora for access to natural sites and for the authorization to collect plant material. We are
711 grateful to the INRA MIGALE bioinformatics platform (<http://migale.jouy.inra.fr>) for providing
712 computational resources and the Genotoul platform for sequencing. We thank the Plateforme de
713 Genotypage GENTYANE INRA UMR1095 for help with microsatellite genotyping. This work

714 was supported by the European Research Council (ERC) (starting grant GenomeFun 309403), the
715 French National Research Agency (ANR) (Gandalf ANR Grant ANR-12-ADAP-0009), the Louis
716 D. Foundation (Institut de France) to TG, and a Marie Curie European grant (PRESTIGE-2016-4-
717 0013) to FEH. PT and CG thank the Région Hauts-de-France, and the Ministère de
718 l'Enseignement Supérieur et de la Recherche (CPER Climibio), and the European Fund for
719 Regional Economic Development for their financial support.

720

721 **Datasets**

722 dataset 1: Hartmann F.E., Snirc A., Cornille A., Godé C., Touzet P., Van Rossum F., Fournier E.,
723 Le Prieur S., Shykoff J., Giraud T. 2019. Plant microsatellite and chloroplastic genotypes. Dryad
724 doi (to be completed upon acceptance).

725 dataset 2: Hartmann F.E., Snirc A., Cornille A., Godé C., Touzet P., Van Rossum F., Fournier E.,
726 Le Prieur S., Shykoff J., Giraud T. 2019. Fungal microsatellite genotypes. Dryad doi (to be
727 completed upon acceptance).

728 dataset 3: Hartmann F.E., Snirc A., Cornille A., Godé C., Touzet P., Van Rossum F., Fournier E.,
729 Le Prieur S., Shykoff J., Giraud T. 2019. Whole genome raw data of *Microbotryum* fungi
730 infecting *S. nutans* and *S. italica*. NCBI Sequence Read Archive (SRA). BioProject xxx (ID
731 available upon acceptance).

732

733

734 **References**

735 Abbate, J. L., Gladieux, P., Hood, M. E., de Vienne, D. M., Antonovics, J., Snirc, A., & Giraud,
736 T. (2018). Co-occurrence among three divergent plant-castrating fungi in the same *Silene*
737 host species. *Molecular Ecology*, 27(16), 3357–3370. doi: 10.1111/mec.14805

738 Antonovics, J., Hood, M. E., & Partain, J. (2002). The ecology and genetics of a host shift:
739 *Microbotryum* as a model system. *The American Naturalist*, 160(S4), S40–S53. doi:
740 10.1086/342143

741 Badouin, H., Gladieux, P., Gouzy, J., Siguenza, S., Aguilera, G., Snirc, A., ... Giraud, T. (2017).
742 Widespread selective sweeps throughout the genome of model plant pathogenic fungi and

- 743 identification of effector candidates. *Molecular Ecology*, 26(7), 2041–2062. doi:
744 10.1111/mec.13976
- 745 Barrès, B., Halkett, F., Dutech, C., Andrieux, A., Pinon, J., & Frey, P. (2008). Genetic structure
746 of the poplar rust fungus *Melampsora larici-populina*: Evidence for isolation by distance
747 in Europe and recent founder effects overseas. *Infection, Genetics and Evolution*, 8(5),
748 577–587. doi: 10.1016/j.meegid.2008.04.005
- 749 Barrett, L. G., Thrall, P. H., Burdon, J. J., & Linde, C. C. (2008). Life history determines genetic
750 structure and evolutionary potential of host–parasite interactions. *Trends in Ecology &
751 Evolution*, 23(12), 678–685. doi: 10.1016/j.tree.2008.06.017
- 752 Becker, R., Wilks, A., Brownrigg, R., Minka, T., & Deckmyn, D. (2017). *maps: draw
753 geographical maps. R package version 3.2.0.* ([https://cran.r-
754 project.org/web/packages/maps/index.html](https://cran.r-project.org/web/packages/maps/index.html)).
- 755 Bernasconi, G., Antonovics, J., Biere, A., Charlesworth, D., Delph, L. F., Filatov, D., ... Widmer,
756 A. (2009). *Silene* as a model system in ecology and evolution. *Heredity*, 103(1), 5–14.
757 doi: 10.1038/hdy.2009.34
- 758 Branco, S., Badouin, H., Rodríguez de la Vega, R. C., Gouzy, J., Carpentier, F., Aguileta, G., ...
759 Giraud, T. (2017). Evolutionary strata on young mating-type chromosomes despite the
760 lack of sexual antagonism. *Proceedings of the National Academy of Sciences*, 114(27),
761 7067–7072. doi: 10.1073/pnas.1701658114
- 762 Branco, S., Carpentier, F., Rodríguez de la Vega, R. C., Badouin, H., Snirc, A., Prieur, S. L., ...
763 Giraud, T. (2018). Multiple convergent supergene evolution events in mating-type
764 chromosomes. *Nature Communications*, 9(1), 2000. doi: 10.1038/s41467-018-04380-9
- 765 Breiman, L. (2001). Random forests. *Machine Learning*, 45(1), 5–32. doi:
766 10.1023/A:1010933404324
- 767 Bucheli, E., Gautschi, B., & Shykoff, J. A. (2000). Host-specific differentiation in the anther
768 smut fungus *Microbotryum violaceum* as revealed by microsatellites. *J. EVOL. BIOL.*, 11.
- 769 Chang, C. C., Chow, C. C., Tellier, L. C., Vattikuti, S., Purcell, S. M., & Lee, J. J. (2015).
770 Second-generation PLINK: rising to the challenge of larger and richer datasets.
771 *GigaScience*, 4(1). doi: 10.1186/s13742-015-0047-8
- 772 Cornille, A., Gladieux, P., Smulders, M. J. M., Roldán-Ruiz, I., Laurens, F., Le Cam, B., ...
773 Giraud, T. (2012). New insight into the history of domesticated apple: Secondary
774 contribution of the European wild apple to the genome of cultivated varieties. *PLOS
775 Genetics*, 8(5), e1002703. doi: 10.1371/journal.pgen.1002703
- 776 Criscione, C. D., Poulin, R., & Blouin, M. S. (2005). Molecular ecology of parasites: elucidating
777 ecological and microevolutionary processes. *Molecular Ecology*, 14(8), 2247–2257. doi:
778 10.1111/j.1365-294X.2005.02587.x
- 779 Croll, D., & Laine, A.-L. (2016). What the population genetic structures of host and pathogen tell
780 us about disease evolution. *New Phytologist*, 212(3), 537–539. doi: 10.1111/nph.14203
- 781 de Vienne, D. M., Hood, M. E., & Giraud, T. (2009). Phylogenetic determinants of potential host
782 shifts in fungal pathogens. *Journal of Evolutionary Biology*, 22(12), 2532–2541. doi:
783 10.1111/j.1420-9101.2009.01878.x
- 784 de Vienne, D. M., Refrégier, G., Hood, M. E., Guigue, A., Devier, B., Vercken, E., ... Giraud, T.
785 (2009). Hybrid sterility and inviability in the parasitic fungal species complex
786 *Microbotryum*. *Journal of Evolutionary Biology*, 22(4), 683–698. doi: 10.1111/j.1420-
787 9101.2009.01702.x
- 788 de Vienne, D. M., Refrégier, G., López-Villavicencio, M., Tellier, A., Hood, M. E., & Giraud, T.
789 (2013). Cospeciation vs host-shift speciation: methods for testing, evidence from natural

- 790 associations and relation to coevolution. *New Phytologist*, 198(2), 347–385. doi:
791 10.1111/nph.12150
- 792 Delmotte, F., Bucheli, E., & Shykoff, J. A. (1999). Host and parasite population structure in a
793 natural plant–pathogen system. *Heredity*, 82(3), 300–308. doi: 10.1046/j.1365-
794 2540.1999.00485.x
- 795 Dray, S., & Dufour, A.-B. (2007). The ade4 Package: Implementing the Duality Diagram for
796 Ecologists. *Journal of Statistical Software*, 22(1), 1–20. doi: 10.18637/jss.v022.i04
- 797 Dybdahl, M. F., & Lively, C. M. (1996). The geography of coevolution: comparative population
798 structures for a snail and its trematode parasite. *Evolution*, 50(6), 2264–2275. doi:
799 10.1111/j.1558-5646.1996.tb03615.x
- 800 Enjalbert, J., Duan, X., Leconte, M., Hovmøller, M. S., & De Vallavieille-Pope, C. (2005).
801 Genetic evidence of local adaptation of wheat yellow rust (*Puccinia striiformis* f. sp.
802 *tritici*) within France. *Molecular Ecology*, 14(7), 2065–2073. doi: 10.1111/j.1365-
803 294X.2005.02566.x
- 804 Estoup, A., Jarne, P., & Cornuet, J.-M. (2002). Homoplasmy and mutation model at microsatellite
805 loci and their consequences for population genetics analysis. *Molecular Ecology*, 11(9),
806 1591–1604. doi: 10.1046/j.1365-294X.2002.01576.x
- 807 Estoup, A., Raynal, L., Verdu, P., & Marin, J.-M. (2018). Model choice using Approximate
808 Bayesian Computation and Random Forests: analyses based on model grouping to make
809 inferences about the genetic history of Pygmy human populations | Journal de la Société
810 Française de Statistique. *Special Issue on Models and Inference in Population Genetics*,
811 159(3). Retrieved from <http://journal-sfds.fr/article/view/709>
- 812 Excoffier, L., & Foll, M. (2011). fastsimcoal: a continuous-time coalescent simulator of genomic
813 diversity under arbitrarily complex evolutionary scenarios. *Bioinformatics*, 27(9), 1332–
814 1334. doi: 10.1093/bioinformatics/btr124
- 815 Excoffier, L., & Lischer, H. E. L. (2010). Arlequin suite ver 3.5: a new series of programs to
816 perform population genetics analyses under Linux and Windows. *Molecular Ecology*
817 *Resources*, 10(3), 564–567. doi: 10.1111/j.1755-0998.2010.02847.x
- 818 Feurtey, A., Gladieux, P., Hood, M. E., Snirc, A., Cornille, A., Rosenthal, L., & Giraud, T.
819 (2016). Strong phylogeographic co-structure between the anther-smut fungus and its
820 white campion host. *New Phytologist*, 212(3), 668–679. doi: 10.1111/nph.14125
- 821 Feurtey, A., & Stukenbrock, E. H. (2018). Interspecific gene exchange as a driver of adaptive
822 evolution in fungi. *Annual Review of Microbiology*, 72(1), 377–398. doi:
823 10.1146/annurev-micro-090817-062753
- 824 Fisher, M. C., Gow, N. A. R., & Gurr, S. J. (2016). Tackling emerging fungal threats to animal
825 health, food security and ecosystem resilience. *Phil. Trans. R. Soc. B*, 371(1709),
826 20160332. doi: 10.1098/rstb.2016.0332
- 827 Fortuna, T. M., Snirc, A., Badouin, H., Gouzy, J., Siguenza, S., Esquerre, D., ... Giraud, T.
828 (2016). Polymorphic microsatellite markers for the tetrapolar anther-smut fungus
829 *Microbotryum saponariae* based on genome sequencing. *PLOS ONE*, 11(11), e0165656.
830 doi: 10.1371/journal.pone.0165656
- 831 Fournier, E., & Giraud, T. (2008). Sympatric genetic differentiation of a generalist pathogenic
832 fungus, *Botrytis cinerea*, on two different host plants, grapevine and bramble. *Journal of*
833 *Evolutionary Biology*, 21(1), 122–132. doi: 10.1111/j.1420-9101.2007.01462.x
- 834 Gandon, S., & Michalakis, Y. (2002). Local adaptation, evolutionary potential and host–parasite
835 coevolution: interactions between migration, mutation, population size and generation
836 time. *Journal of Evolutionary Biology*, 15(3), 451–462. doi: 10.1046/j.1420-

- 837 9101.2002.00402.x
- 838 Gandon, S., Capowiez, Y., Dubois, Y., Michalakakis, Y., & Olivieri, I. (1996). Local adaptation
839 and gene-for-gene coevolution in a metapopulation model. *Proceedings of the Royal*
840 *Society of London. Series B: Biological Sciences*, 263(1373), 1003–1009. doi:
841 10.1098/rspb.1996.0148
- 842 Gerritsen, H. (2013). *Mapplots, r package version 1.5*. [https://CRAN.R-](https://CRAN.R-project.org/package=mapplots)
843 [project.org/package=mapplots](https://CRAN.R-project.org/package=mapplots).
- 844 Gibson, A. K., Hood, M. E., & Giraud, T. (2012). Sibling competition arena: selfing and a
845 competition arena can combine to constitute a barrier to gene flow in sympatry. *Evolution*,
846 66(6), 1917–1930. doi: 10.1111/j.1558-5646.2011.01563.x
- 847 Giraud, T. (2004). Patterns of within population dispersal and mating of the fungus
848 *Microbotryum violaceum* parasitising the plant *Silene latifolia*. *Heredity*, 93(6), 559–565.
849 doi: 10.1038/sj.hdy.6800554
- 850 Giraud, T., & Gourbière, S. (2012). The tempo and modes of evolution of reproductive isolation
851 in fungi. *Heredity*, 109(4), 204–214. doi: 10.1038/hdy.2012.30
- 852 Giraud, T., Yockteng, R., Marthey, S., Chiapello, H., Jonot, O., Lopez-Villavicencio, M., ...
853 Dossat, C. (2008). Isolation of 60 polymorphic microsatellite loci in EST libraries of four
854 sibling species of the phytopathogenic fungal complex *Microbotryum*. *Molecular Ecology*
855 *Resources*, 8(2), 387–392. doi: 10.1111/j.1471-8286.2007.01967.x
- 856 Gladieux, P., Devier, B., Aguilera, G., Cruaud, C., & Giraud, T. (2013). Purifying selection after
857 episodes of recurrent adaptive diversification in fungal pathogens. *Infection, Genetics and*
858 *Evolution: Journal of Molecular Epidemiology and Evolutionary Genetics in Infectious*
859 *Diseases*, 17, 123–131. doi: 10.1016/j.meegid.2013.03.012
- 860 Gladieux, P., Vercken, E., Fontaine, M. C., Hood, M. E., Jonot, O., Couloux, A., & Giraud, T.
861 (2011). Maintenance of fungal pathogen species that are specialized to different hosts:
862 allopatric divergence and introgression through secondary contact. *Molecular Biology and*
863 *Evolution*, 28(1), 459–471. doi: 10.1093/molbev/msq235
- 864 Godé, C., Touzet, P., Martin, H., Lahiani, E., Delph, L. F., & Arnaud, J.-F. (2014).
865 Characterization of 24 polymorphic microsatellite markers for *Silene nutans*, a
866 gynodioecious–gynomonoecious species, and cross-species amplification in other *Silene*
867 species. *Conservation Genetics Resources*, 6(4), 915–918. doi: 10.1007/s12686-014-
868 0240-6
- 869 Hafner, M. S., Page, R. D. M. (1995). Molecular phylogenies and host-parasite cospeciation:
870 gophers and lice as a model system. *Philosophical Transactions of the Royal Society of*
871 *London. Series B: Biological Sciences*, 349(1327), 77–83. doi: 10.1098/rstb.1995.0093
- 872 Hartmann, F. E., Rodríguez de la Vega, R. C., Brandenburg, J.-T., Carpentier, F., & Giraud, T.
873 (2018). Gene presence–absence polymorphism in castrating anther-smut fungi: recent
874 gene gains and phylogeographic structure. *Genome Biology and Evolution*, 10(5), 1298–
875 1314. doi: 10.1093/gbe/evy089
- 876 Hartmann, F. E., Rodríguez de la Vega, R. C., Carpentier, F., Gladieux, P., Cornille, A., Hood,
877 M. E., & Giraud, T. (2019). Understanding adaptation, coevolution, host specialization,
878 and mating system in castrating anther-smut fungi by combining population and
879 comparative genomics. *Annual Review of Phytopathology*, 57(1), 431–457. doi:
880 10.1146/annurev-phyto-082718-095947
- 881 Hood, M. E., Antonovics, J., Wolf, M., Stern, Z. L., Giraud, T., & Abbate, J. L. (2019). Sympatry
882 and interference of divergent *Microbotryum* pathogen species. *Ecology and Evolution*,
883 0(0). doi: 10.1002/ece3.5140

- 884 Huson, D. H. (1998). SplitsTree: analyzing and visualizing evolutionary data. *Bioinformatics*
885 (Oxford, England), 14(1), 68–73.
- 886 Huson, D. H., & Bryant, D. (2006). Application of phylogenetic networks in evolutionary studies.
887 *Molecular Biology and Evolution*, 23(2), 254–267. doi: 10.1093/molbev/msj030
- 888 Jakobsson, M., & Rosenberg, N. A. (2007). CLUMPP: a cluster matching and permutation
889 program for dealing with label switching and multimodality in analysis of population
890 structure. *Bioinformatics*, 23(14), 1801–1806. doi: 10.1093/bioinformatics/btm233
- 891 Jombart, T. (2008). adegenet: a R package for the multivariate analysis of genetic markers.
892 *Bioinformatics*, 24(11), 1403–1405. doi: 10.1093/bioinformatics/btn129
- 893 Jombart, T., & Ahmed, I. (2011). adegenet 1.3-1: new tools for the analysis of genome-wide SNP
894 data. *Bioinformatics*, 27(21), 3070–3071. doi: 10.1093/bioinformatics/btr521
- 895 Jürgens, A., Witt, T., & Gottsberger, G. (1996). Reproduction and pollination in central European
896 populations of *Silene* and *Saponaria* species. *Botanica Acta*, 109(4), 316–324. doi:
897 10.1111/j.1438-8677.1996.tb00579.x
- 898 Kaltz, O., Gandon, S., Michalakis, Y., & Shykoff, J. A. (1999). Local maladaptation in the
899 anther-smut fungus *Microbotryum violaceum* to its host plant *Silene latifolia*: evidence
900 from a cross-inoculation experiment. *Evolution; International Journal of Organic*
901 *Evolution*, 53(2), 395–407. doi: 10.1111/j.1558-5646.1999.tb03775.x
- 902 Keenan, K., McGinnity, P., Cross, T. F., Crozier, W. W., & Prodöhl, P. A. (2016). diveRsity: An
903 R package for the estimation and exploration of population genetics parameters and their
904 associated errors. *Methods in Ecology and Evolution*, 782–788. doi: 10.1111/2041-
905 210X.12067@10.1111/(ISSN)2041-210X.ecologyandevolutionireland
- 906 Kemler, M., Göker, M., Oberwinkler, F., & Begerow, D. (2006). Implications of molecular
907 characters for the phylogeny of the Microbotryaceae (Basidiomycota: Urediniomycetes).
908 *BMC Evolutionary Biology*, 6, 35. doi: 10.1186/1471-2148-6-35
- 909 Kephart, S., Reynolds, R. J., Rutter, M. T., Fenster, C. B., & Dudash, M. R. (2006). Pollination
910 and seed predation by moths on *Silene* and allied Caryophyllaceae: evaluating a model
911 system to study the evolution of mutualisms. *New Phytologist*, 169(4), 667–680. doi:
912 10.1111/j.1469-8137.2005.01619.x
- 913 Lafuma, L., & Maurice, S. (2006). Reproductive characters in a gynodioecious species, *Silene*
914 *italica* (Caryophyllaceae), with attention to the gynomonoeious phenotype. *Biological*
915 *Journal of the Linnean Society*, 87(4), 583–591. doi: 10.1111/j.1095-8312.2006.00597.x
- 916 Lahiani, E., Dufaÿ, M., Castric, V., Le Cadre, S., Charlesworth, D., Van Rossum, F., & Touzet,
917 P. (2013). Disentangling the effects of mating systems and mutation rates on cytoplasmic
918 diversity in gynodioecious *Silene nutans* and dioecious *Silene otites*. *Heredity*, 111(2),
919 157–164. doi: 10.1038/hdy.2013.32
- 920 Laine, A.-L. (2005). Spatial scale of local adaptation in a plant-pathogen metapopulation. *Journal*
921 *of Evolutionary Biology*, 18(4), 930–938. doi: 10.1111/j.1420-9101.2005.00933.x
- 922 Laine, A.-L. (2008). Temperature-mediated patterns of local adaptation in a natural plant-
923 pathogen metapopulation. *Ecology Letters*, 11(4), 327–337. doi: 10.1111/j.1461-
924 0248.2007.01146.x
- 925 Laine, A.-L., Barrès, B., Numminen, E., & Siren, J. P. (2019). Variable opportunities for
926 outcrossing result in hotspots of novel genetic variation in a pathogen metapopulation.
927 *ELife*, 8. doi: 10.7554/eLife.47091
- 928 Langmead, B., Trapnell, C., Pop, M., & Salzberg, S. L. (2009). Ultrafast and memory-efficient
929 alignment of short DNA sequences to the human genome. *Genome Biology*, 10(3), R25.
930 doi: 10.1186/gb-2009-10-3-r25

- 931 Le Gac, M., Hood, M. E., Fournier, E., & Giraud, T. (2007). Phylogenetic evidence of host-
932 specific cryptic species in the anther smut fungus. *Evolution; International Journal of*
933 *Organic Evolution*, *61*(1), 15–26. doi: 10.1111/j.1558-5646.2007.00002.x
- 934 Le Gac, M., Hood, M. E., & Giraud, T. (2007). Evolution of reproductive isolation within a
935 parasitic fungal species complex. *Evolution*, *61*(7), 1781–1787. doi: 10.1111/j.1558-
936 5646.2007.00144.x
- 937 Linde, C. C., Zhan, J., & McDonald, B. A. (2002). Population structure of *Mycosphaerella*
938 *graminicola*: from lesions to continents. *Phytopathology*, *92*(9), 946–955. doi:
939 10.1094/PHYTO.2002.92.9.946
- 940 Liu, S., Cornille, A., Decroocq, S., Tricon, D., Chague, A., Eyquard, J.-P., ... Decroocq, V.
941 (2019). From hybrid speciation of wild *Armeniaca* species to multiple domestication
942 events in Eastern Asia: the complex evolutionary history of apricots. *Under Review*.
- 943 López-Villavicencio, M., Jonot, O., Coantic, A., Hood, M. E., Enjalbert, J., & Giraud, T. (2007).
944 Multiple infections by the anther smut pathogen are frequent and involve related strains.
945 *PLOS Pathogens*, *3*(11), e176. doi: 10.1371/journal.ppat.0030176
- 946 Lutz, M., Göker, M., Piatek, M., Kemler, M., Begerow, D., & Oberwinkler, F. (2005). Anther
947 smuts of Caryophyllaceae: Molecular characters indicate host-dependent species
948 delimitation. *Mycological Progress*, *4*(3), 225–238. doi: 10.1007/s11557-006-0126-4
- 949 Martin, M. (2011). Cutadapt removes adapter sequences from high-throughput sequencing reads.
950 *EMBnet Journal*, *17*(1), 10–12. doi: 10.14806/ej.17.1.200
- 951 Martin, H., Touzet, P., Dufay, M., Godé, C., Schmitt, E., Lahiani, E., ... Rossum, F. V. (2017).
952 Lineages of *Silene nutans* developed rapid, strong, asymmetric postzygotic reproductive
953 isolation in allopatry. *Evolution*, *71*(6), 1519–1531. doi: 10.1111/evo.13245
- 954 Martin, H., Touzet, P., Van Rossum, F., Delalande, D., & Arnaud, J.-F. (2016). Phylogeographic
955 pattern of range expansion provides evidence for cryptic species lineages in *Silene nutans*
956 in Western Europe. *Heredity*, *116*(3), 286–294. doi: 10.1038/hdy.2015.100
- 957 McCoy, K. D., Boulinier, T., & Tirard, C. (2005). Comparative host–parasite population
958 structures: disentangling prospecting and dispersal in the black-legged kittiwake *Rissa*
959 *tridactyla*. *Molecular Ecology*, *14*(9), 2825–2838. doi: 10.1111/j.1365-
960 294X.2005.02631.x
- 961 McDonald, B. A., & Stukenbrock, E. H. (2016). Rapid emergence of pathogens in agro-
962 ecosystems: global threats to agricultural sustainability and food security. *Phil. Trans. R.*
963 *Soc. B*, *371*(1709), 20160026. doi: 10.1098/rstb.2016.0026
- 964 McKenna, A., Hanna, M., Banks, E., Sivachenko, A., Cibulskis, K., Kernytsky, A., ... DePristo,
965 M. A. (2010). The Genome Analysis Toolkit: a MapReduce framework for analyzing
966 next-generation DNA sequencing data. *Genome Research*, *20*(9), 1297–1303. doi:
967 10.1101/gr.107524.110
- 968 Michalakis, Y., Sheppard, A. W., Noel, V., & Olivieri, I. (1993). Population structure of a
969 herbivorous insect and its host plant on a microgeographic scale. *Evolution*, *47*(5), 1611–
970 1616. doi: 10.2307/2410172
- 971 Naciri, Y., Pasquier, P.-E. D., Lundberg, M., Jeanmonod, D., & Oxelman, B. (2017). A
972 phylogenetic circumscription of *Silene* sect. *Siphonomorpha* (Caryophyllaceae) in the
973 Mediterranean Basin. *Taxon*, *66*(1), 91–108. doi: 10.12705/661.5
- 974 Nei, M. (1972). Genetic distance between populations. *The American Naturalist*, *106*(949), 283–
975 292. doi: 10.1086/282771
- 976 Nieberding, C. M., Durette-Desset, M.-C., Vanderpoorten, A., Casanova, J. C., Ribas, A.,
977 Deffontaine, V., ... Michaux, J. R. (2008). Geography and host biogeography matter for

- 978 understanding the phylogeography of a parasite. *Molecular Phylogenetics and Evolution*,
979 47(2), 538–554. doi: 10.1016/j.ympev.2008.01.028
- 980 Nieberding, C. M., & Olivieri, I. (2007). Parasites: proxies for host genealogy and ecology?
981 *Trends in Ecology & Evolution*, 22(3), 156–165. doi: 10.1016/j.tree.2006.11.012
- 982 Paradis, E., Claude, J., & Strimmer, K. (2004). APE: Analyses of Phylogenetics and Evolution in
983 R language. *Bioinformatics*, 20(2), 289–290. doi: 10.1093/bioinformatics/btg412
- 984 Petit, E., Silver, C., Cornille, A., Gladieux, P., Rosenthal, L., Bruns, E., ... Hood, M. E. (2017).
985 Co-occurrence and hybridization of anther-smut pathogens specialized on *Dianthus* hosts.
986 *Molecular Ecology*, 26(7), 1877–1890. doi: 10.1111/mec.14073
- 987 Piry, S., Luikart, G., & Cornuet, J. M. (1999). *BOTTLENECK: A computer program for detecting*
988 *recent reductions in the effective population size using allele frequency data*. 90, 502–
989 503.
- 990 Poulin, R. (2005). *Parasite biodiversity*. Smithsonian Institution.
- 991 Pritchard, J. K., Stephens, M., & Donnelly, P. (2000). Inference of population structure using
992 multilocus genotype data. *Genetics*, 155(2), 945–959.
- 993 Pudlo, P., Marin, J.-M., Estoup, A., Cornuet, J.-M., Gautier, M., & Robert, C. P. (2016). Reliable
994 ABC model choice via random forests. *Bioinformatics*, 32(6), 859–866. doi:
995 10.1093/bioinformatics/btv684
- 996 Purcell, S., Neale, B., Todd-Brown, K., Thomas, L., Ferreira, M. A. R., Bender, D., ... Sham, P.
997 C. (2007). PLINK: A tool set for whole-genome association and population-based linkage
998 analyses. *The American Journal of Human Genetics*, 81(3), 559–575. doi:
999 10.1086/519795
- 1000 Rameau, J.-C., Mansion, D., & Dumé, G. (1989). *Flore forestière française: Plaines et collines*.
1001 Forêt privée française.
- 1002 Rameau, J.-C., Mansion, D., & Dumé, G. (2008). *Flore forestière française: guide écologique*
1003 *illustré. Région méditerranéenne*. Forêt privée française.
- 1004 Raynal, L., Marin, J.-M., Pudlo, P., Ribatet, M., Robert, C. P., & Estoup, A. (2019). ABC random
1005 forests for Bayesian parameter inference. *Bioinformatics*, 35(10), 1720–1728. doi:
1006 10.1093/bioinformatics/bty867
- 1007 Refrégier, G., Le Gac, M., Jabbour, F., Widmer, A., Shykoff, J. A., Yockteng, R., ... Giraud, T.
1008 (2008). Cophylogeny of the anther smut fungi and their Caryophyllaceae hosts:
1009 prevalence of host shifts and importance of delimiting parasite species for inferring
1010 cospeciation. *BMC Evolutionary Biology*, 8, 100. doi: 10.1186/1471-2148-8-100
- 1011 Saleh, D., Milazzo, J., Adreit, H., Fournier, E., & Tharreau, D. (2014). South-East Asia is the
1012 center of origin, diversity and dispersion of the rice blast fungus, *Magnaporthe oryzae*.
1013 *New Phytologist*, 201(4), 1440–1456. doi: 10.1111/nph.12627
- 1014 Stukenbrock, E. H., Banke, S., & McDonald, B. A. (2006). Global migration patterns in the
1015 fungal wheat pathogen *Phaeosphaeria nodorum*. *Molecular Ecology*, 15(10), 2895–2904.
1016 doi: 10.1111/j.1365-294X.2006.02986.x
- 1017 Stukenbrock, E. H., & McDonald, B. A. (2008). The origins of plant pathogens in agro-
1018 ecosystems. *Annual Review of Phytopathology*, 46(1), 75–100. doi:
1019 10.1146/annurev.phyto.010708.154114
- 1020 Szpiech, Z. A., Jakobsson, M., & Rosenberg, N. A. (2008). ADZE: a rarefaction approach for
1021 counting alleles private to combinations of populations. *Bioinformatics*, 24(21), 2498–
1022 2504. doi: 10.1093/bioinformatics/btn478
- 1023 Taylor, D. R., & Keller, S. R. (2007). Historical range expansion determines the phylogenetic
1024 diversity introduced during contemporary species invasion. *Evolution*, 61(2), 334–345.

- 1025 doi: 10.1111/j.1558-5646.2007.00037.x
1026 Tellier, A., de Vienne, D. M., Giraud, T., Hood, M. E., & Refrégier, G. (2010). Theory and
1027 examples of reciprocal influence between hosts and pathogens, from short-term to long
1028 term interactions: coevolution, cospeciation and pathogen speciation following host shifts.
1029 In *Immunology and Immune System Disorders. Host-Pathogen Interactions: Genetics,*
1030 *Immunology and Physiology* (Nova Science Publishers, pp. 37–77). NY: Barton AW.
1031 Thines, M. (2019). An evolutionary framework for host shifts – jumping ships for survival. *New*
1032 *Phytologist*, 224(2), 605–617. doi: 10.1111/nph.16092
1033 Thompson, J. N. (2005). *The geographic mosaic of coevolution*. University of Chicago Press.
1034 Thrall, P., Biere, A., & Antonovics, J. (1993). Plant life-history and disease susceptibility - the
1035 occurrence of Ustilago-Violacea on different species within the Caryophyllaceae. *Journal*
1036 *of Ecology*, 81(3), 489–498. doi: 10.2307/2261527
1037 Tison, J., & de Foucault, B. (2014). *Flora gallica: flore de France* (Biotope).
1038 Toh, S. S., & Perlin, M. H. (2016). Resurgence of less-studied smut fungi as models of
1039 phytopathogenesis in the omics age. *Phytopathology*, 106(11), 1244–1254. doi:
1040 10.1094/PHYTO-02-16-0075-RVW
1041 Tsai, Y.-H. E., & Manos, P. S. (2010). Host density drives the postglacial migration of the tree
1042 parasite, *Epifagus virginiana*. *Proceedings of the National Academy of Sciences*, 107(39),
1043 17035–17040. doi: 10.1073/pnas.1006225107
1044 Tutin, T., Heywood, V., Burges, N., Valentine, D., Walters, S., & Webb, D. (2001). *Flora*
1045 *Europaea*. Royaume-Uni: Cambridge University Press.
1046 Van Rossum, F., Martin, H., Le Cadre, S., Brachi, B., Christenhusz, M. J. M., & Touzet, P.
1047 (2018). Phylogeography of a widely distributed species reveals a cryptic assemblage of
1048 distinct genetic lineages needing separate conservation strategies. *Perspectives in Plant*
1049 *Ecology, Evolution and Systematics*, 35, 44–51. doi: 10.1016/j.ppees.2018.10.003
1050 Vercken, E., Fontaine, M. C., Gladieux, P., Hood, M. E., Jonot, O., & Giraud, T. (2010). Glacial
1051 refugia in pathogens: European genetic structure of anther smut pathogens on *Silene*
1052 *latifolia* and *Silene dioica*. *PLOS Pathogens*, 6(12), e1001229. doi:
1053 10.1371/journal.ppat.1001229
1054 Wegmann, D., Leuenberger, C., Neuenschwander, S., & Excoffier, L. (2010). ABCtoolbox: a
1055 versatile toolkit for approximate Bayesian computations. *BMC Bioinformatics*, 11(1), 116.
1056 doi: 10.1186/1471-2105-11-116
1057 Wickham, H. (2009). *ggplot2: elegant graphics for data analysis*. Springer Science & Business
1058 Media.
1059 Wilson, D. J., Falush, D., & McVean, G. (2005). Germs, genomes and genealogies. *Trends in*
1060 *Ecology & Evolution*, 20(1), 39–45. doi: 10.1016/j.tree.2004.10.009
1061 Wolfe, N. D., Dunavan, C. P., & Diamond, J. (2007). Origins of major human infectious diseases.
1062 *Nature*, 447(7142), 279–283. doi: 10.1038/nature05775
1063 Zaffarano, P. L., McDonald, B. A., & Linde, C. C. (2008). Rapid speciation following recent host
1064 shifts in the plant pathogenic fungus *Rhynchosporium*. *Evolution*, 62(6), 1418–1436. doi:
1065 10.1111/j.1558-5646.2008.00390.x
1066

1067 **Data accessibility**

1068 The plant and fungal microsatellite and chloroplastic genotypes are available at dryad XXX (to
1069 be completed upon acceptance). We deposited the genome raw data at NCBI Sequence Read
1070 Archive (SRA) under the BioProject xxx (ID available upon acceptance).

1071

1072 **Author contributions**

1073 TG and FH conceived and designed the project with the help of FVR. TG, PT, FVR, JS and EF
1074 collected samples. AS, CG, PT, SLP and FH genotyped the samples. FH and AC performed the
1075 analyses. FH, TG and FVR wrote the manuscript. All authors read and approved the final version
1076 of the manuscript and declare no conflict of interest.

1077

1078

1079 **Supporting information**

1080 Additional Supporting Information may be found in the online version of this article.

1081

1082

1083 **Tables**

1084 **Table 1: Comparisons of scenarios and group of scenarios used for approximate Bayesian**
1085 **computation (ABC) to reconstruct the fungi divergence history.** Scenarios are described in
1086 Table S5 and Fig S5. Results of ABC random forest procedure are shown, with the percentage of
1087 vote for each scenario/group of scenarios, the posterior probability and the prior error rate.

1088

ABC round	Tested hypothesis	Number of tested scenarios/group of scenarios	Description of tested scenarios/group of scenarios	Best scenario/group of scenarios	Percentage of vote	Posterior probability	Prior error rate in %
Round 1: "time of divergence"	divergence time T1, T2, T3 or T4	4 groups of 3 scenarios	group 1 (time T1): divergence-order-A-no-GF-T1, divergence-order-B-no-GF-T1, divergence-order-C-no-GF-T1 group 2 (time T2): divergence-order-A-no-GF-T2, divergence-order-B-no-GF-T2, divergence-order-C-no-GF-T2 group 3 (time T3): divergence-order-A-no-GF-T3, divergence-order-B-no-GF-T3, divergence-order-C-no-GF-T3 group 4 (time T4): divergence-order-A-no-GF-T4, divergence-order-B-no-GF-T4, divergence-order-C-no-GF-T4	x	1 5 43 51	0.54 (+-0.02)	34%
Round 2: "divergence order"	Order of divergence A, B or C	3 scenarios	scenario 1 (order A): divergence-order-A-no-GF-T4 scenario 2 (order B): divergence-order-B-no-GF-T4 scenario 3 (order C): divergence-order-C-no-GF-T4	x	80 5 15	0.79 (+-0.02)	2%
Round 3: "occurrence of gene flow"	step1: absence of gene flow, or gene flow between nutans clusters only or gene flow with the outgroup	3 groups of 1, 6 and 6 scenarios	group 1 (no gene flow): divergence-order-A-no-GF-T4 group 2 (gene flow between nutans clusters only): divergence-order-A-T4-GF1, divergence-order-A-T4-GF3, divergence-order-A-T4-GF5, divergence-order-A-T4-GF6, divergence-order-A-T4-GF10, divergence-order-A-T4-GF12 group 3 (gene flow with the outgroup): divergence-order-A-T4-GF2, divergence-order-A-T4-GF4, divergence-order-A-T4-GF7, divergence-order-A-T4-GF8, divergence-order-A-T4-GF9, divergence-order-A-T4-GF11	x	33 42 24	0.60 (+-0.02)	5%
	step2: continuous gene flow, secondary contact or ancient migration	3 groups of 3, 2 and 4 scenarios	group 1 (continuous gene flow): divergence-order-A-T4-GF1, divergence-order-A-T4-GF5, divergence-order-A-T4-GF6 group 2 (secondary contact): divergence-order-A-T4-GF3, divergence-order-A-T4-GF3b group 3 (ancient migration): divergence-order-A-T4-GF10, divergence-order-A-T4-GF10b, divergence-order-A-T4-GF12, divergence-order-A-T4-GF12b	x	23 3 74	0.76 (+-0.02)	35%
	step3: absence of gene flow vs ancient migration	2 groups of 1 and 4 scenarios	group 1 (no gene flow): divergence-order-A-no-GF-T4 group 2 (ancient migration): divergence-order-A-T4-GF10, divergence-order-A-T4-GF10b, divergence-order-A-T4-GF12, divergence-order-A-T4-GF12b	x	34 66	0.66 (+-0.02)	2.50%
	step4: absence of gene flow vs secondary contact	2 groups of 1 and 3 scenarios	group 1 (no gene flow): divergence-order-A-no-GF-T4 group 2 (secondary contact): divergence-order-A-T4-GF3, divergence-order-A-T4-GF3b	x	99 1	0.99 (+-0.004)	0.76%
	step5: comparison of different scenarios of ancient migration	4 scenarios	scenario 1: divergence-order-A-T4-GF10 scenario 2: divergence-order-A-T4-GF10b scenario 3: divergence-order-A-T4-GF12 scenario 4: divergence-order-A-T4-GF12b	x	29 24 26 21	0.49 (+-0.03)	60%

1089

1090 **Figures**

1091 **Figure 1: Population genetic structure of *Silene nutans* and *S. italica* host plants based on**
1092 **six plastid (chloroplast) SNPs and 21 microsatellite markers.** A. Plastid haplotypes according
1093 to their geographic distribution. On the right, a zoom of the map in the northeastern region of
1094 France and Belgium is shown. The size of the symbols is proportional to the number of
1095 individuals sampled by site (1-9 plants). B. Principal component analysis (PCA), with
1096 information of plastid haplotypes. The first and second principal component axes are shown and
1097 the percentage of variance explained by each axis is indicated into brackets. C. Results of
1098 STRUCTURE on both host plant species for K=5 clusters. On panels A and B, symbol shape
1099 indicates species and color indicates plastid haplotypes. The two genetic clusters identified within
1100 the orange plastid haplotype based on the STRUCTURE analysis (panel C) are shown with light
1101 and dark orange colors, respectively.

1102

1103 **Figure 2: Population genetic structure of anther-smut fungi (*Microbotryum*) parasitizing**
1104 ***Silene nutans* and *S. italica* based on 22 microsatellite markers.** A. Anther-smut fungi
1105 parasitizing *S. italica* (top; photo credit M.E. Hood) and *S. nutans* (bottom; photo credit M.
1106 Strack van Schijndel). B. Principal component analysis (PCA). The first and second principal
1107 component axes are shown and the percentage of variance explained by each axis is indicated
1108 into brackets. The symbol shape indicates the sampling host species. The dark and light blue
1109 colors indicate assignment probability >0.80 to the two corresponding clusters identified in the
1110 STRUCTURE analysis for K=2 (see panel C). Pink color indicates strains for which no cluster
1111 could be assigned with a probability >0.80. Genetic variance explained by the principal
1112 component axes is shown in the right bottom corner. C. STRUCTURE barplot for K=2. Strains
1113 are ordered according to their sampling host species.

1114

1115 **Figure 3: Congruence of population genetic structure between *Silene nutans* host plants and**
1116 **their anther-smut fungal (*Microbotryum*) strains based on microsatellite markers.** A.
1117 Principal component analysis (PCA) on the fungal strains with information of the population
1118 genetic structure of their hosts. The first and second principal component axes are shown.
1119 Symbol shape indicates the sampling host species and color indicates the plastid haplotypes of
1120 the sampling host. B. STRUCTURE barplots for (1) K=3 in 112 *Microbotryum* strains and (2)
1121 K=4 in 110 *S. nutans* plant individuals. Fungal strains are ordered according to their sampling
1122 host plastid haplotypes. Host plant individuals are ordered according to their plastid haplotypes.
1123 C. Map of mean cluster membership proportions per site for (1) the 112 fungal strains in the
1124 STRUCTURE analysis at K=3 and (2) the 110 *S. nutans* plant individuals in the STRUCTURE
1125 analysis at K=4. The pie diameter reflects the sample size in the corresponding site (1 - 14
1126 individuals).

1127

1128 **Figure 4: Most likely scenario for the divergence between the fungal genetic clusters**
1129 **inferred with approximate Bayesian computation (ABC).**

1130

1131 **Figure 5: Absence of genome-wide signature of recent gene flow among anther-smut fungal**
1132 **strains parasitizing closely related *Silene* species.** A. Principal component analysis (PCA)
1133 based on 1,305,369 genome-wide SNPs. B. STRUCTURE analyses based on 233 unlinked SNPs
1134 for $K=5$. The Y axis indicates the estimated membership proportions in the K clusters for each
1135 fungal strain (X axis). C. Neighbornet tree from a SplitsTree analysis based on 595,002 genome-
1136 wide SNPs with no missing data and heterozygote genotypes. The inner plot shows a zoom of the
1137 tip of the tree for strains parasitizing *S. nutans*. Information on the species or plastid haplotype of
1138 the host of sampling of the strains is given.

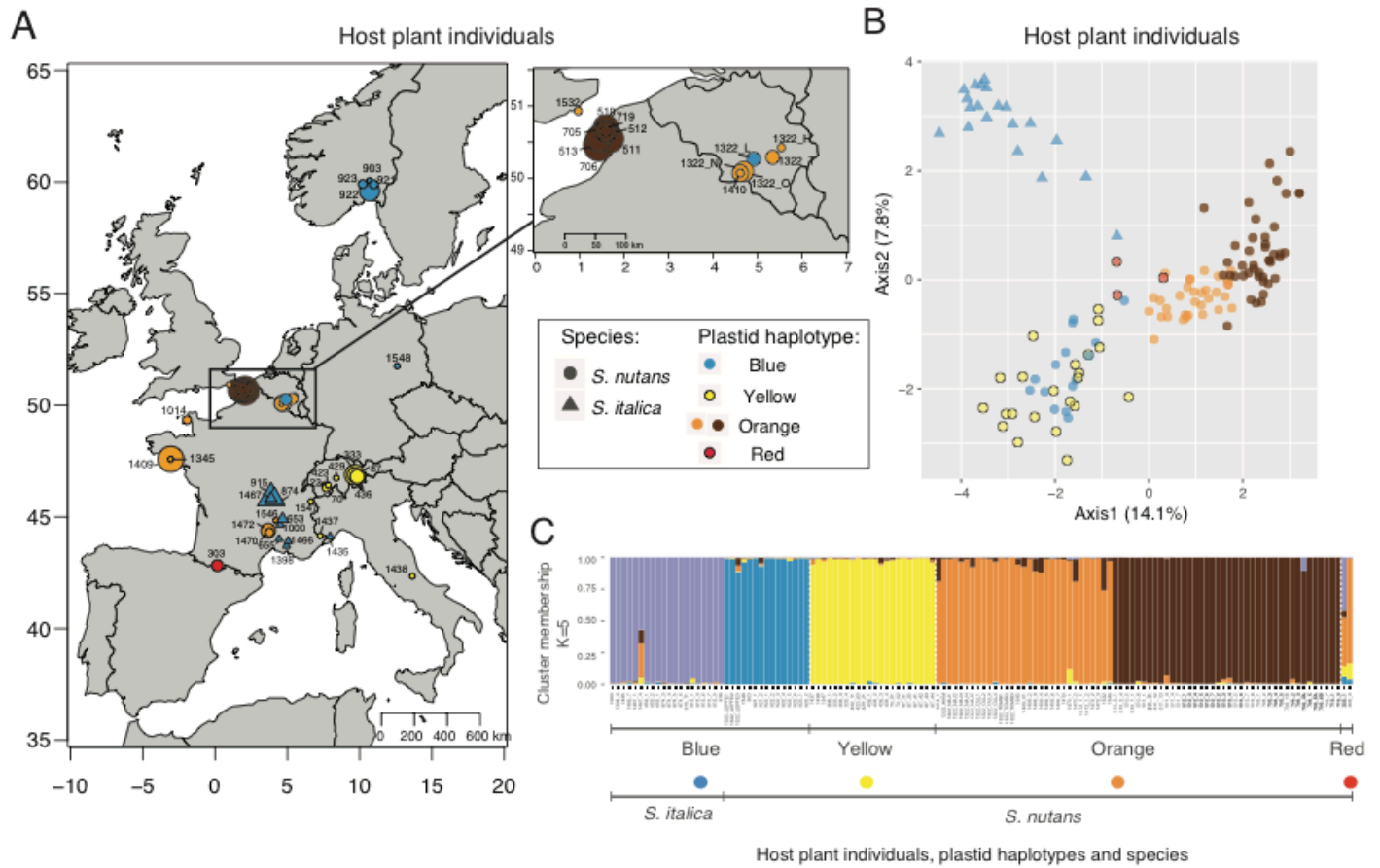


Figure 1

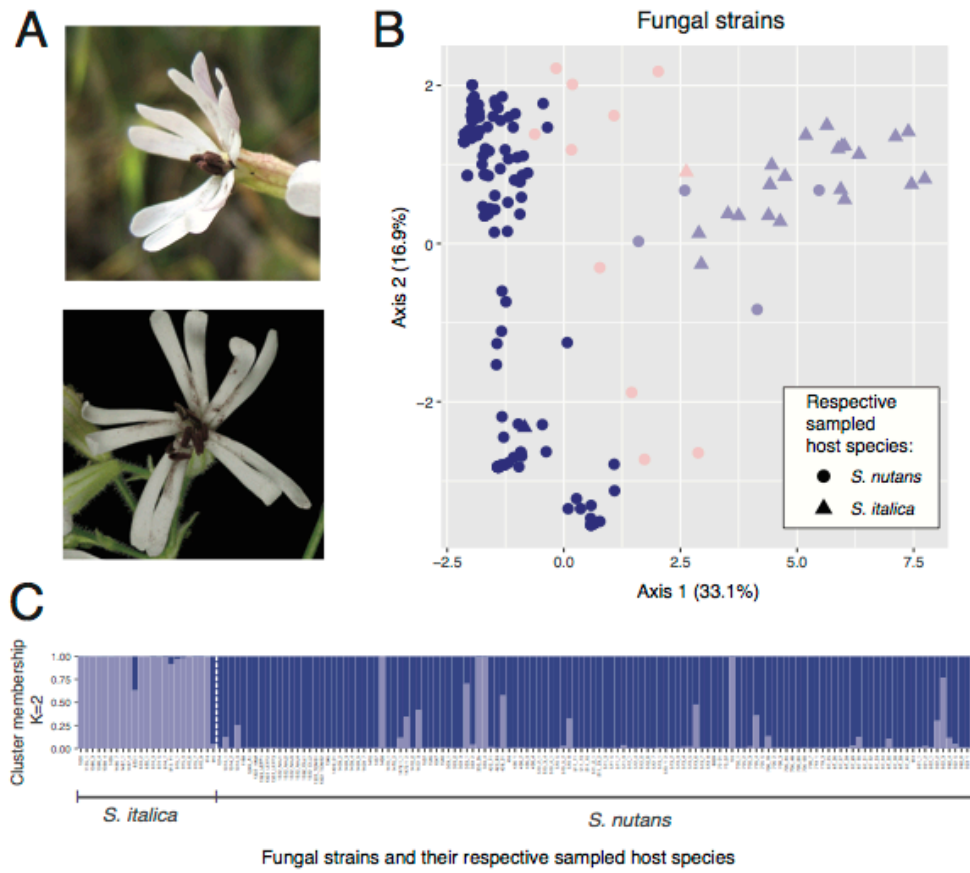


Figure 2

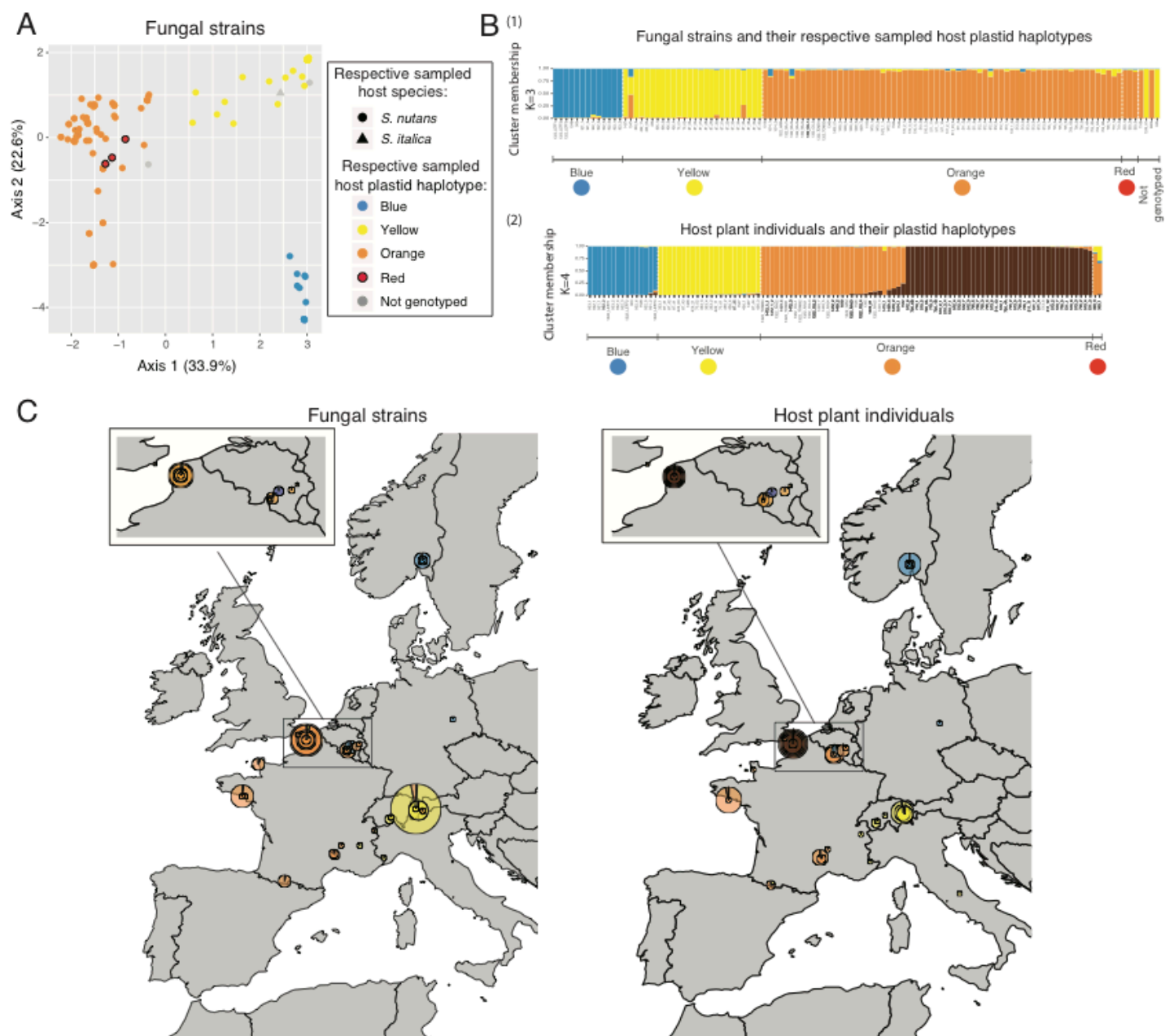


Figure 3

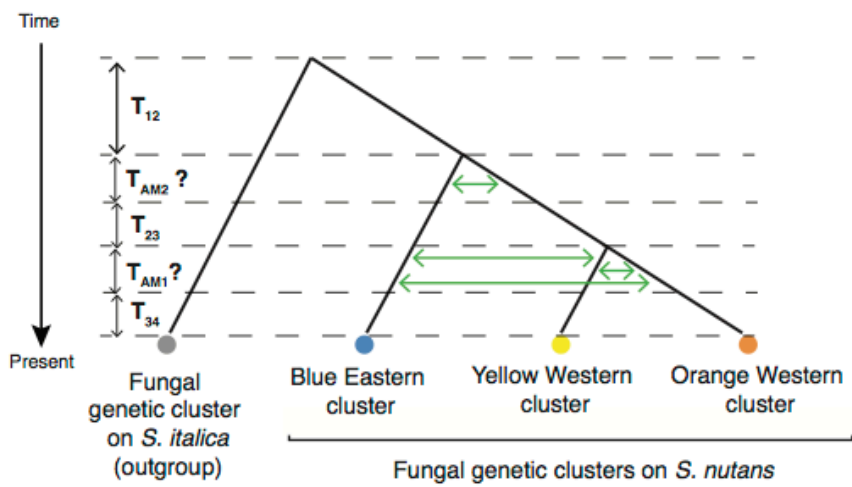


Figure 4

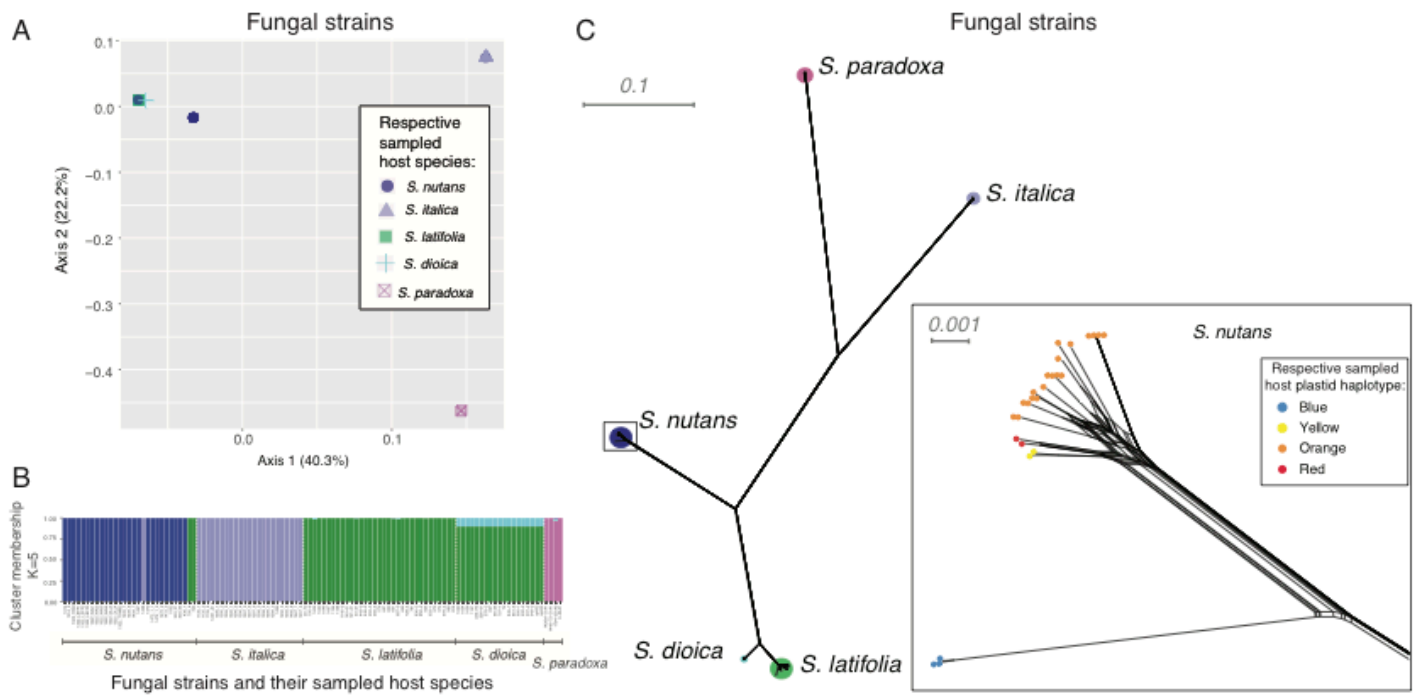


Figure 5